

1 **CD8⁺ T-cell responses are boosted by dual PD-1/VEGFR2 blockade after EGFR**

2 **inhibition in *Egfr*-mutant lung cancer**

3

4 **Authors and affiliations:**

5 ¹Kazuya Nishii, MD, ^{2*}Kadoaki Ohashi, MD, PhD, ³Shuta Tomida, PhD, ¹Takamasa
6 Nakasuka, MD, ¹Atsuko Hirabae, MD, ¹Sachi Okawa, MD, ¹Jun Nishimura, MD, ¹Hisao
7 Higo, MD, PhD, ¹Hiroshi Watanabe, MD, PhD, ¹Hirohisa Kano, MD, PhD, ¹Chihiro
8 Ando, MD, ¹Go Makimoto, MD, PhD, ¹Kiichiro Ninomiya, MD, PhD, ⁴Yuka Kato,
9 MD, PhD, ⁵Toshio Kubo, MD, PhD, ²Eiki Ichihara, MD, PhD, ⁴Katsuyuki Hotta, MD,
10 PhD, MPH, ⁵Masahiro Tabata, MD, PhD, ⁶Shinichi Toyooka, MD, PhD, ⁷Heiichiro
11 Uono, MD, PhD, ¹Yoshinobu Maeda, MD, PhD, ²Katsuyuki Kiura, MD, PhD

12

13 1 Department of Hematology, Oncology and Respiratory Medicine, Okayama
14 University Graduate School of Medicine, Dentistry and Pharmaceutical Sciences,
15 Okayama, Japan
16 2 Department of Respiratory Medicine, Okayama University Hospital, Okayama, Japan.
17 3. Center for Comprehensive Genomic Medicine, Okayama University Hospital,
18 Okayama, Japan
19 4. Center of Innovative Clinical Medicine, Okayama University Hospital, Okayama,
20 Japan
21 5. Center for Clinical Oncology, Okayama University Hospital, Okayama, Japan
22 6. Department of General Thoracic Surgery and Breast and Endocrinological Surgery,
23 Okayama University Graduate School of Medicine, Dentistry, and Pharmaceutical
24 Sciences, Okayama, Japan.
25 7. Department of Immunology, Okayama University Graduate School of Medicine,
26 Dentistry and Pharmaceutical Sciences, Okayama, Japan

27 **Running title:** CD8⁺ T cell-dependent responses in *Egfr*-mutant lung cancer

28

29 **Funding:**

30 This work was supported by a specific grant from JSPS Grant-in-Aid for Scientific
31 Research [Scientific Research (C): KAKEN 19K08625 to K.O. and K.K.], JSPS Grants-
32 in-Aid for Scientific Research [Scientific Research (B): KAKEN 19H03667 to K.K.,
33 S.T. and K.O.] and JSPS Grants-in-Aid for Scientific Research [Scientific Research (B):
34 KAKEN 22H03078 to K.O., S.T. and K.K.]. This work was also supported by Ryobi
35 Teien Memory Foundation (K.O.), and The Okayama Medical Foundation (K.O.)

36

37 ***Corresponding author:** Kadoaki Ohashi, MD, PhD.

38 Okayama University Graduate School of Medicine, Dentistry and Pharmaceutical
39 Sciences, Department of Hematology, Oncology and Respiratory Medicine
40 2-5-1 Shikata-cho, Kita-ku, Okayama, 700-8558, Japan
41 PHONE: +81-86-235-7227,
42 FAX: +81-86-232-8226,
43 E-mail: kohashi@cc.okayama-u.ac.jp

44

45 **Conflicts of interest:**

46 Dr Kadoaki Ohashi received honoraria from Boehringer Ingelheim, Novartis, and
47 Chugai pharmaceutical; research funding from Boehringer Ingelheim, Novartis,
48 AstraZeneca, Eli Lilly, MSD, and Daiichi-Sankyo outside the submitted work. Dr
49 Kiichiro Ninomiya received honoraria from AstraZeneca, Boehringer Ingelheim, Eli
50 Lilly, MSD, Ono Pharmaceutical, Nippon Kayaku, Taiho pharmaceutical, Kyowa-Kirin,
51 and Chugai pharmaceutical outside the submitted work. Dr Katsuyuki Hotta received
52 honoraria from AstraZeneca and MSD; research funding from Chugai Pharmaceutical,
53 Eli Lilly Japan, Bristol-Myers Squibb, Astellas Pharma and AstraZeneca outside the

CD8⁺ T cell-dependent response in *Egfr*-mutant lung cancer

54 submitted work. Dr Katsuyuki Kiura received honoraria from MSD; research funding
55 from Ono Pharmaceutical, Boehringer Ingelheim, Taiho Pharmaceutical, Chugai
56 Pharmaceutical, Nippon Kayaku, Bristol-Myers Squibb, and Shionogi & Co., Ltd.,
57 outside the submitted work.

58

59 **Key Words:** lung adenocarcinoma, EGFR tyrosine kinase inhibitor, anti-PD-1, anti-
60 VEGFR2, CD8-positive T cells

61

62 **Abstract**

63 Epidermal growth factor receptor (*EGFR*) is the most frequently mutated driver
64 oncogene in non-smoking-related, non-small-cell lung cancer (NSCLC). *EGFR*-mutant
65 NSCLC has a non-inflamed tumor microenvironment (TME), with low infiltration by
66 CD8⁺ T cells and, thus, immune checkpoint inhibitors, such as anti-programmed cell
67 death-1 (anti-PD-1) have weak anti-tumor effects. Here, we showed that CD8⁺ T-cell
68 responses were induced by an EGFR-tyrosine kinase inhibitor (TKI) in syngeneic *Egfr*-
69 mutant NSCLC tumors, which was further pronounced by sequential dual blockade of
70 PD-1 and vascular endothelial growth factor receptor 2 (VEGFR2). However,
71 simultaneous triple blockade had no such effect. PD-1/VEGFR2 dual blockade did not
72 exert tumor-inhibitory effects without pre-treatment with the EGFR-TKI, suggesting
73 that treatment schedule is crucial for efficacy of the dual blockade therapy. Pre-
74 treatment with EGFR-TKI increased the CD8⁺ T-cell/regulatory T-cell (Treg) ratio,
75 while also increasing expression of immunosuppressive chemokines and chemokine
76 receptors, as well as increasing the number of M2-like macrophages, in the TME.
77 Discontinuing EGFR-TKI treatment reversed the transient increase of
78 immunosuppressive factors in the TME. The subsequent PD-1/VEGFR2 inhibition
79 maintained increased numbers of infiltrating CD8⁺ T cells and CD11c⁺ dendritic cells.

CD8⁺ T cell-dependent response in *Egfr*-mutant lung cancer

80 Depletion of CD8⁺ T cells *in vivo* abolished tumor growth inhibition by EGFR-TKI
81 alone and the sequential triple therapy, suggesting that EGFR inhibition is a prerequisite
82 for the induction of CD8⁺ T-cell responses. Our findings could aid in developing an
83 alternative immunotherapy strategy in patients with cancers that have driver mutations
84 and a non-inflamed TME.

85

86 **Synopsis**

87 *Egfr*-mutant lung cancer exhibits a non-inflamed tumor microenvironment (TME).
88 Here, data demonstrate that the scheduling of EGFR inhibition with dual PD-
89 1/VEGFR2 blockade is vital for optimum efficacy and induction of CD8⁺ T cell-
90 dominant responses in the TME.

91 **Introduction**

92 Immune checkpoint inhibitors (ICIs), such as antibodies targeting programmed cell
93 death-1 (PD-1) or programmed death-ligand 1 (PD-L1), have revolutionized cancer
94 treatment and demonstrated to improve overall survival in patients with advanced
95 malignant diseases, including non-small-cell lung cancers (NSCLCs) (1). However,
96 ICIs have exerted little effect in NSCLCs harboring non-smoking-related oncogenes,
97 such as epidermal growth factor receptor (*EGFR*) mutations or anaplastic lymphoma
98 kinase (*ALK*) fusion genes (2,3). The low number of CD8⁺ T cells infiltrating tumors
99 (i.e., non-inflamed tumor) or lower tumor mutation burden is considered to be a reason
100 underlying the poor effect of ICIs in NSCLC with non-smoking-related oncogenes (4).
101 Therefore, a novel immunotherapeutic strategy is required to provide a survival benefit
102 for patients with this particular subtype of NSCLC.

103 *EGFR* gene mutations are the most frequently detected driver oncogene mutations in
104 non-smoking-related NSCLCs (5,6). Inhibition of the oncoprotein with EGFR-tyrosine
105 kinase inhibitors (TKIs) produce a transient cancer inhibition; however, resistance
106 inevitably develops within two years due to genetic or non-genetic alterations *EGFR*-
107 mutant NSCLCs (7–10). A study has revealed that oncogenic EGFR signaling is
108 involved not only in tumorigenesis, but also in the formation of an immune-suppressive

109 tumor microenvironment (TME) in lung cancer (4). However, combination therapies
110 with EGFR-TKIs and anti-PD-1/PD-L1 or anti-cytotoxic T lymphocyte associated
111 antigen-4 (CTLA-4) demonstrate an insufficient inhibitory effect and raises concerns
112 about toxicity in clinical trials (11–15). Similar results have been reported for *ALK*
113 fusion gene-positive lung cancer (11,14).

114 Several pre-clinical studies have suggested the involvement of the vascular
115 endothelial growth factor (VEGF)/VEGF receptor-2 (VEGFR2) pathway in the
116 tolerogenic immune responses (16). Combination therapies with EGFR-TKIs and
117 VEGF/VEGFR2 inhibitors have been tested in multiple clinical trials and have shown a
118 significant prolongation in progression-free survival in patients with *EGFR*-mutant lung
119 cancers (17,18). However, none of the clinical trials showed a benefit in overall
120 survival, suggesting that the activation of tumor immunity might be insufficient. In
121 contrast, combination therapy with ICIs and VEGF or VEGFR2 inhibitors have been
122 shown to improve survival in several solid cancers, including NSCLC (19–21).
123 Nevertheless, the role of dual blockade of the PD-1 and VEGFR2 pathways has not
124 been fully established in lung cancer harboring *EGFR* mutations.

125 Currently, there are few *in vivo* preclinical models that can be used to assess the
126 effect of ICIs in lung cancer harboring *EGFR* mutations. Thus, we previously

127 established genetically engineered mouse lung cancer models harboring *EGFR*
128 mutations using the SP-C promoter in immunocompetent C57BL/6 mice (22,23). These
129 mice spontaneously develop EGFR-dependent lung adenocarcinoma from type II
130 pneumocytes. We also established a syngeneic mouse model via subcutaneous
131 transplantation of the spontaneously originating lung tumor cells into wild-type
132 C57BL/6 mice (24). In this study, we employed these tumor models and assessed the
133 dynamic changes in the TME of lung tumors harboring *Egfr* mutation and investigated
134 the effect of combined immunotherapy using an EGFR-TKI, anti-PD-1, and/or anti-
135 VEGFR2.

136

137 **Methods**

138 **Reagents and antibodies**

139 For *in vivo* experiments in syngeneic *Egfr*-mutant lung -cancer mouse model (described
140 below), gefitinib or afatinib were purchased from Everlth (Hiroshima, Japan), and
141 FTY720 was purchased from Cayman Chemical (Michigan, IL, USA, catalog no.
142 10006292). Additional treatments of tumor-bearing mice (described below) included:
143 anti-VEGFR2 (clone DC101: rat monoclonal IgG1 κ), mouse IgG1 isotype control
144 (clone MOPC-21: mouse IgG1 κ), and rat IgG1 isotype control (clone HRPN: rat IgG1 κ)

CD8⁺ T cell-dependent response in *Egfr*-mutant lung cancer

145 were purchased from BioXcell (Lebanon, NH, USA); anti-PD-1 (clone 4H2: mouse
146 monoclonal IgG1 κ) was provided by Ono Pharmaceutical Co., Ltd. under material
147 transfer agreement (Osaka, Japan); and anti-CD8 α (clone 53-6.7: rat monoclonal
148 IgG2 $\alpha\kappa$) and rat IgG2a isotype control (clone RTK2758: rat IgG2 $\alpha\kappa$) were purchased
149 from BioLegend (San Diego, CA, USA). The following primary antibodies for
150 immunohistochemistry (IHC; described below) were used: anti-CD8 α (EPR21769) was
151 purchased from Abcam (Cambridge, UK); anti-FasL (bs-0216R) was purchased from
152 Bioss Antibodies (Woburn, MA, USA); anti-Foxp3 (D608R), anti-CD11c (D1V9Y),
153 anti-CD31 (D8V9E), anti-CD206 (E6T5J), anti-VEGFR2 (55B11), anti-PD-L1
154 (D5V3B), and anti-PD-L2 (D6L5A) were purchased from Cell Signaling Technology
155 (Danvers, MA, USA). The EnVision+System-labeled polymer-horseradish peroxidase
156 anti-rabbit antibody (Dako, Glostrup, Denmark. catalog no. K4002) was used as the
157 secondary antibody for the IHC. The Liquid DAB⁺ Substrate Chromogen System was
158 used for DAB (3,3'-Diaminobenzidine) staining (Dako, catalog no. K3468). Flow
159 cytometry (FCM; described below) antibodies: anti-CD8 α (53-6.7), anti-CD4 (GK1.5),
160 anti-CD25 (PC61.5), anti-CD3 (17A2), anti-Foxp3 (FJK-16s), anti-PD-1 (RMP1-30),
161 anti-H-2kb (AF6-88.5.5.3), and mouse IgG2a (eBM2a) were purchased from Thermo
162 Fisher Scientific (Waltham, MA, USA); antibodies against PD-L1 (10F.9G2), PD-L2

CD8⁺ T cell-dependent response in *Egfr*-mutant lung cancer

163 (TY25), H-2Db (KH95), and CD107a (1D4B) were purchased from BioLegend;
164 Zombie Violet (catalog no. 423113) and antibodies against rat IgG2b (RTK4530), rat
165 IgG2a (RTK2758), and mouse IgG2a (MPC-11) were purchased from BioLegend;
166 interferon alpha (IFN α) or interferon gamma (IFN γ) were purchased from Miltenyi
167 Biotec (Bergisch Gladbach, Germany, catalog no. 130-093-131) or BioLegend (catalog
168 no. 575302) respectively.

169

170 **Cell lines**

171 MC-38 murine colon adenocarcinoma cells (catalog no. KER-ENH204) were purchased
172 from Kerafast (Boston, MA, USA) in 2019 for this study. The cell lines were
173 authenticated by Kerafast ([https://www.kerafast.com/productgroup/665/mc-38-cell-](https://www.kerafast.com/productgroup/665/mc-38-cell-line)
174 [line](https://www.kerafast.com/productgroup/665/mc-38-cell-line)). The number of cell passages was five times after the purchase. The cell lines were
175 verified as mycoplasma free before starting the experiments (iNtRON Biotechnology,
176 Inc. Seongnam, Korea, catalog no. 25237). MC38 cells were cultured in Dulbecco's
177 modified MEM(DMEM)(Sigma-Aldrich, catalog no. D6429) with 10% fetal bovine
178 serum (Thermo Fisher, catalog no. 10270-1061), 1% penicillin-streptomycin (Thermo
179 Fisher, catalog no. 15140-22). Cells were incubated in a humidified incubator with 5%
180 CO₂ at 37 °C.

181

182 **PD-L1 and PD-L2 expression on *Egfr*-mutant tumor cells or MC-38 cells**

183 The subcutaneous *Egfr*-mutated lung tumor was minced and dissociated into single-cell
184 suspensions by using a Tumor Dissociation Kit, mouse (Miltenyi Biotec, catalog no.
185 130-096-730) (described below). 5×10^5 *Egfr*-mutant tumor cells or 1×10^5 of MC38
186 cells were incubate in 3ml of DMEM with 10% FBS, 1% Penicillin-Streptomycin in
187 6well plate (Corning, New York, NY, USA, catalog no. 353046) in a humidified
188 incubator with 5% CO₂ at 37 °C for 3 days. IFN- α (Miltenyi Biotec catalog no. 130-
189 093-131. 5×10^2 U/ml), or IFN- γ (BioLegend catalog no. 575302. 1×10^2 U/ml) were
190 added 24 hours before assessed the cells with anti-PD-L1 (Thermo Fisher Scientific,
191 10F.9G2) or anti-PD-L2 (Thermo Fisher Scientific, TY25) via FCM as described
192 below. DMEM was added as vehicle control for IFN- α or IFN- γ . As isotype control, rat
193 IgG2b (BioLegend, RTK4530) or rat IgG2a (BioLegend, RTK2758) were used for anti-
194 PD-L1 or anti-PD-L2 respectively.

195

196 **Tumor models**

197 Syngeneic *Egfr*-mutant lung-cancer mouse model: Female C57BL/6J mice aged 6–8
198 weeks were purchased from Charles River Laboratories Japan, Inc. (Yokohama, Japan).

CD8⁺ T cell-dependent response in *Egfr*-mutant lung cancer

199 All mice were provided with sterilized food and water and were housed in a barrier
200 facility, maintained at an air-conditioned temperature of $22 \pm 2^{\circ}\text{C}$, with constant
201 humidity under a 12/12-hour light/dark cycle. The mice were monitored twice a week.
202 Subcutaneous tumors harboring *Egfr* exon 19 deletions were passaged using C57BL/6J
203 mice prepared basically as described previously (24). For this study, the subcutaneous
204 *Egfr*-mutated lung tumor was minced and dissociated into single-cell suspensions by
205 using a Tumor Dissociation Kit, mouse (Miltenyi Biotec, catalog no. 130-096-730)
206 (described below), and then red blood cells were removed from the suspensions by
207 using the Red Blood Cell Lysis Solution (Miltenyi Biotec, catalog no. 130-094-183).
208 The suspension solution of 1×10^6 tumor cells in 0.1 mL of PBS mixed with 0.1 mL of
209 Matrigel matrix (Corning, catalog no. 356237) were prepared per 1 tumor, and injected
210 into the double flanks of the mice unless otherwise specified in the figure legend. When
211 the average volume of transplanted tumors reached approximately 200 mm^3 5 to 7 days
212 after the subcutaneous transplantation, the mice were randomly assigned to groups and
213 treated with saline (Otsuka, catalog no. 87-3311) with 0.5% polyoxyethylene sorbitan
214 monooleate (nacalai tesque, catalog no. 35703-75) as the vehicle, gefitinib (5–50
215 mg/kg/day, administered by oral gavage [p.o.], 5 or 7 days/week for 14 days or 21
216 days), afatinib (15 mg/kg/day, administered by oral gavage [p.o.], 7 days/week for 14

CD8⁺ T cell-dependent response in *Egfr*-mutant lung cancer

217 days), FTY720 (300 µg/kg/day, administered by oral gavage [p.o.], 7 days/week for 12
218 days), or anti-VEGFR2 (10 mg/kg/day, injected intraperitoneally [i.p.], every 3 days for
219 7 days), rat IgG1 isotype control (BioXcell, clone HRPN: rat IgG1κ) for anti-VEGFR2,
220 anti-PD-1 (10 mg/kg/day, i.p., every 5 days for 18 days), mouse IgG1 isotype control
221 (BioXcell, clone MOPC-21: mouse IgG1κ) for anti-PD-1, combination of gefitinib (50
222 mg/kg/day, administered by oral gavage [p.o.], 7 days/week for 18 days) and FTY720
223 (300 µg/kg/day, administered by oral gavage [p.o.], 7 days/week for 18 days),
224 combination of gefitinib (50 mg/kg/day, administered by oral gavage [p.o.], 5
225 days/week for 14 days) and anti-PD-1(10 mg/kg/day, injected intraperitoneally [i.p.],
226 every 5 days for 14 days), combination of gefitinib (50 mg/kg/day, administered by oral
227 gavage [p.o.], 5 days/week for 14 days) and anti-VEGFR2 antibody (10 mg/kg/day,
228 injected intraperitoneally [i.p.], every 3 days for 14 days), combination of anti-PD-1 (10
229 mg/kg/day, injected intraperitoneally [i.p.], every 3 days for 10 days) and ant-VEGFR2
230 (10 mg/kg/day, injected intraperitoneally [i.p.], every 3 days for 10 days), the sequential
231 therapy with prior gefitinib monotherapy (50 mg/kg/day, administered by oral gavage
232 [p.o.], 7 days/week for 14 days) followed by anti-PD-1 (10 mg/kg/day, injected
233 intraperitoneally [i.p.], every 3 days for 7 days), ant-VEGFR2 (10 mg/kg/day, injected
234 intraperitoneally [i.p.], every 3 days for 7 days) or combination of anti-PD-1 (10

CD8⁺ T cell-dependent response in *Egfr*-mutant lung cancer

235 mg/kg/day, injected intraperitoneally [i.p.], every 3 days for 7 days) and anti-VEGFR2
236 (10 mg/kg/day, injected intraperitoneally [i.p.], every 3 days for 7 days) , the
237 concomitant triple therapy with gefitinib (50 mg/kg/day, administered by oral gavage
238 [p.o.], 5 days/week for 14 days), anti-PD-1(10 mg/kg/day, injected intraperitoneally
239 [i.p.], every 5 days for 14 days) and anti-VEGFR2 (10 mg/kg/day, injected
240 intraperitoneally [i.p.], every 3 days for 14 days), or late concomitant triple therapy with
241 prior gefitinib monotherapy (50 mg/kg/day, administered by oral gavage [p.o.], 7
242 days/week for 14 days) and followed by the triple therapy gefitinib (50 mg/kg/day,
243 administered by oral gavage [p.o.], 7 days/week for 7 days), anti-PD-1(10 mg/kg/day,
244 i.p., every 5 days for 7 days) and anti-VEGFR2 (10 mg/kg/day, injected
245 intraperitoneally [i.p.], every 3 days for 7 days). Tumors were collected at day 3 from the
246 mice treated with gefitinib monotherapy, the combination of gefitinib and anti-PD-1,
247 combination of gefitinib and anti-VEGFR2, combination of anti-PD-1 and anti-
248 VEGFR2. Tumors were also harvested from the mice treated with gefitinib
249 monotherapy or combination of gefitinib and FTY720 at day7, the mice treated with
250 gefitinib monotherapy at day 14, or the mice treated with sequential therapies of prior
251 gefitinib monotherapy followed by vehicle, anti-PD-1, anti-VEGFR2 or the
252 combination of anti-PD-1 and anti-VEGFR2 at day 21. Spleen was harvested the mice

CD8⁺ T cell-dependent response in *Egfr*-mutant lung cancer

253 treated with vehicle for 3 days. For the depletion of CD8⁺ T cells, either anti-mouse
254 CD8 α (250 μ g/injection, injected intraperitoneally [i.p.]) or IgG2a isotype control (250
255 μ g/injection, injected intraperitoneally [i.p.]) were administered on day 0 and day 3, and
256 then once weekly until the end of the study (day 28 for the tumor treated with gefitinib
257 monotherapy, day 35 for the tumors treated with sequential therapy of prior gefitinib
258 followed by combination of anti-PD-1 and anti-VEGFR2) . The tumor volume ($\text{width}^2 \times$
259 $\text{length}/2$) was determined periodically by caliper measurements twice a week. The
260 experimental protocol was approved by the Animal Care and Use Committee of
261 Okayama University, Okayama, Japan (OKU-2020228). Mice were kept on study until
262 tumors reached 2,000 mm³, or the study reached the termination point at day 14, day 21,
263 day 28 or day 35.

264 Subcutaneous MC-38 model:

265 Female C57BL/6J mice aged 6–8 weeks were purchased from Charles River
266 Laboratories Japan, Inc. All mice were provided with sterilized food and water and were
267 housed in a barrier facility, maintained at an air-conditioned temperature of $22 \pm 2^\circ\text{C}$,
268 with constant humidity under a 12/12-hour light/dark cycle. The mice were monitored
269 twice a week. A total of 2×10^5 MC38 cells were injected subcutaneously into the
270 single flank and monitored for tumor growth. The tumor volume ($\text{width}^2 \times \text{length}/2$)

271 was determined periodically by caliper measurements twice a week. Mice were treated
272 intraperitoneally with anti-PD-1 (10 mg/kg/day, injected intraperitoneally [i.p.], every 5
273 days for 24 days) post tumor transplant. For controls, mice were injected with 200 µg of
274 IgG1 antibody (BioXcell, clone MOPC-21: mouse IgG1κ). The experimental protocol
275 was approved by the Animal Care and Use Committee of Okayama University,
276 Okayama, Japan (OKU-2020228). Mice were kept on study until tumors reached 2,000
277 mm³, or the study reached the termination point at day 24.

278

279 **Tissue dissociation into single-cell suspensions**

280 Tumor tissues were dissected from the mice and dissociated into single-cell
281 suspensions using a Tumor Dissociation Kit mouse (Miltenyi Biotec, catalog no. 130-
282 096-730), according to the manufacturer's protocol. The grafted *Egfr* mutated tumors
283 were removed from subcutaneous, cut into 2-4 mm size, and put in gentle MACS C
284 Tubes with enzyme mixed solution. The solution was prepared by adding 2.35 mL of
285 RPMI 1640 (Sigma-Aldrich, catalog no. R8758), 100 µL of Enzyme D, 50 µL of
286 Enzyme R, and 12.5 µL of Enzyme A. The dissociation was performed using the
287 program (37c_m_TDK_1) with gentle MACS Octo Dissociator with Heaters
288 (Miltenyi Biotec, catalog no. 130-096-427). After the dissociation, the solution was

CD8⁺ T cell-dependent response in *Egfr*-mutant lung cancer

289 processed with Red Blood Cell Lysis Solution (Miltenyi Biotec, catalog no. 130-
290 094-183). Tumors were collected at day 3 from the mice treated with gefitinib
291 monotherapy, anti-PD-1, anti-VEGFR2, the combination of gefitinib and anti-PD-1,
292 combination of gefitinib and anti-VEGFR2, combination of anti-PD-1 and anti-
293 VEGFR2. Tumors were also harvested from the mice treated with gefitinib
294 monotherapy at day 14.

295

296 **RNA extraction**

297 RNA was extracted from the lungs of 12-week-old *Egfr* mutated transgenic mice or
298 wild type C57BL/6J mice without treatment, or subcutaneously grafted *Egfr* mutated
299 tumors treated with saline with 0.5% polyoxyethylene sorbitan monooleate as vehicle
300 for 3 days, gefitinib for 3 days or 14 days, prior gefitinib for 14 days followed by
301 isotype control antibody, anti-PD-1, anti-VEGFR2, or the combination of anti-PD-1 and
302 anti-VEGFR2 for 7 days using the RNeasy Mini Kit (Qiagen, Venlo, The Netherlands)
303 according to the manufacturer's protocol. Extracted RNA was used for mRNA profiling
304 as described below.

305

306 **Targeted gene expression profiling using NanoString**

CD8⁺ T cell-dependent response in *Egfr*-mutant lung cancer

307 Targeted mRNA expression profiling was conducted on the extracted RNA from the
308 lung of *Egfr* mutant transgenic mice or wild type mice using the NanoString nCounter
309 gene expression platform (NanoString Technologies, Seattle, WA, USA) and the
310 PanCancer Mouse Immune Profiling gene expression panel (NanoString Technologies).
311 nCounter analysis was performed by RIKEN GENESIS (Kanagawa, Japan), according
312 to the manufacturer's protocol. For each sample, 200 ng of RNA was hybridized to the
313 probes included in the PanCancer Mouse Immune Profiling gene expression panel and
314 processed according to the manufacturer's protocols. A custom probe was not used for
315 the analysis. The preparation was performed using nCounter Master Kit (NanoString
316 Technologies, catalog no. NAA-AKIT-012) at 65°C for 16 hours with T100 Thermal
317 Cycler (Bio-Rad, catalog no. 186-1096). The cartridge containing purified RNA hybrids
318 was analyzed via nCounter FLEX Analysis System (NanoString Technologies). The
319 raw count data (RCC files) were log₂-transformed and normalized to housekeeping
320 genes using default protocols and settings of nSolver 4.0 software provided by
321 NanoString Technologies. nSolver software was used for quality control and
322 normalization of the primary data. Advanced Analysis function in nSolver was not used
323 for this study. The data were used to calculate "Relative gene expression Score"
324 between the lung of transgenic mice and wild-type mice. "Relative gene expression

325 Score” was calculated by averaging the relative expression of the genes in each immune
326 response category. Immune response categories including “Adaptive”, “Innate”,
327 “Leukocyte Function”, “T Cell Functions”, “B Cell Functions”, “NK Cell Functions”,
328 “Dendric cell functions”, “Macrophage Functions”, “Mast cell function”, “Interferon”,
329 “Interleukins”, “Cytokines and Receptors”, and “Chemokines and Receptors” were
330 defined and annotated based on gene list under the “Support Documentation” for “Panel
331 Gene Lists” of nCounter PanCancer Mouse Immune Profiling provided by NanoString
332 Technologies (<https://nanosttring.com/support/support-documentation/#h-panel-gene->
333 lists). Hierarchical clustering was performed and displayed by using cluster 3.0
334 (<http://bonsai.hgc.jp/~mdehoon/software/cluster/software.htm>) and Java treeview
335 (<http://jtreeview.sourceforge.net/>) .

336

337 **mRNA expression profiling using next-generation sequencing**

338 rRNA was depleted from extracted RNA from the tumors of syngeneic *Egfr*-mutant
339 lung cancer mouse model using the NEBNext rRNA Depletion Kit v2
340 (Human/Mouse/Rat; E7405, New England Biolabs Japan Inc., Tokyo, Japan). cDNA
341 libraries were prepared using the MGIEasy RNA Directional Library Prep Set (MGI
342 Tech Japan, Tokyo, Japan). RNA-sequencing (RNA-seq) was performed on a

343 DNBSEQ-G400RS sequencer (MGI Tech Co., Ltd., Shanghai, China) using DNBSEQ-
344 G400RS High throughput Sequencing Set (MGI Tech Co., Ltd., Shanghai, catalog no.
345 FCL PE150) with the 150-base paired-end setting. Sequencing data were mapped onto
346 the mouse reference genome (Genome Reference Consortium Mouse Build 38 patch
347 release 6) and normalized to calculate TPM (transcripts per million) values for protein
348 coding genes using the CLC Genomics Workbench (CLC bio, Aarhus, Denmark).
349 Reads counts (number of reads) were divided by the length of each gene in kilobases
350 (reads per kilobase; RPK). Then, all of the RPKs for protein coding genes were counted
351 up (sum of RPK). Finally, RPK were normalized by dividing the following scaling
352 factor ((sum of RPK)/1,000,000). In this process, all read counts were used (i.e. the
353 threshold for read count was not set) to calculate TPM. quanTIseq analyses using the
354 TPM data were performed via TIMER2.0 according to the tutorial
355 (<http://timer.cistrome.org/>)(25,26).

356

357 **Immunohistochemistry (IHC)**

358 IHC was conducted using the tumors of syngeneic *Egfr*-mutant lung cancer mouse
359 model as described previously (27,28). Formalin-fixed, paraffin-embedded tissues were
360 cut to a thickness of 5 μ m, placed on glass slides, and deparaffinized as follows: rinse 3

CD8⁺ T cell-dependent response in *Egfr*-mutant lung cancer

361 times in Hemo-De (FALMA, Tokyo, Japan, catalog no. CS-1001-4) for 5 minutes, and
362 then soaked in 99.5% ethanol (Sigma-Aldrich, catalog no. 09-0770-5) for 2 min, 95%
363 ethanol for 2 minutes, 70% ethanol for 2 minutes and pure water for 3 minutes. The
364 slides were incubated in pure water containing 1 mM EDTA (Invitrogen, catalog no.
365 15575-020) for 10 min in a 95 °C Pascal (Dako, catalog no. S2800) and soaked in 0.3%
366 hydrogen peroxide (SANTOKU CHEMICAL, Tokyo, Japan, catalog no. 18412) with
367 methanol (nacalai tesque, catalog no. 21915-93) as solvent to inactivate endogenous
368 peroxidase for 5 minutes. The slides were rinsed with Tris Buffered Saline (TBS, pure
369 water containing 20 mM trizma base [Sigma-Aldrich, catalog no: T1503], 137 mM
370 NaCL [Sigma-Aldrich, catalog no: 28-2270-5] and adjusted to pH 7.0 with HCL
371 [nacalai tesque, catalog no. 37338-15]) with 0.1% polyoxyethylene sorbitan
372 monolaurate (nacalai tesque, catalog no. 35624-15) and the sections were incubated
373 with 240 µl of wash buffer (Dako, catalog no. S3006) and 30 µl of goat serum
374 (Invitrogen, catalog no. 01-6201) for 60 min at room temperature. CD8 α (Abcam,
375 EPR21769), Foxp3 (Cell Signaling Technology, D608R) anti-CD11c (Cell Signaling
376 Technology, D1V9Y), anti-PD-L1 (Cell Signaling Technology, D5V3B), anti-PD-L2
377 (Cell Signaling Technology, D6L5A), anti-CD31 (Cell Signaling Technology, D8V9E),
378 anti-VEGFR2 (Cell Signaling Technology, 55B11), anti-FasL (Bioss Antibodies, bs-

CD8⁺ T cell-dependent response in *Egfr*-mutant lung cancer

379 0216R) antibodies were diluted at 1/2000, 1/100, 1/350, 1/200, 1/200, 1/100, 1/600 and
380 1/200 respectively. Anti-CD206 (Cell Signaling Technology, E6T5J) was diluted to
381 1µg/ml. Rabbit IgG (Cell Signaling Technology, DA1E) was diluted at 1/2000 and used
382 as isotype antibody. Dako wash buffer was used for the dilution (Dako, catalog no.
383 S3006). The sections were incubated overnight at 4°C with primary antibodies
384 (specified above), followed by incubation with a secondary antibody (Dako, catalog no.
385 K4003. 1/1 Undiluted) for 20 minutes at room temperature. Finally, DAB staining was
386 performed using Liquid DAB+ Substrate Chromogen System (Dako, catalog no.
387 K3468) and the sections were counterstained with hematoxylin (MUTO PURE
388 CHEMICALS, Tokyo, Japan, catalog no: 30002). The microscope (KEYENCE, Osaka,
389 Japan, catalog no. BZ8100) was used for assessment. Percentage of DAB positive area
390 was measured using ImageJ software (version 1.52a). DAB positive areas were isolated
391 using the color deconvolution plugin (Vectors: H-DAB). The threshold value was
392 manually set to match the DAB-positive areas. In this study, the threshold value (30-
393 125) was applied to the images. Each image was changed into a binary (black and
394 white) color image before the measurement. Tumor tissues were collected at day 3 from
395 the mice treated with saline with 0.5% polyoxyethylene sorbitan monooleate as vehicle,
396 gefitinib monotherapy, anti-VEGFR2, combination of gefitinib and anti-VEGFR2.

397 Tumor tissues were also harvested from the mice treated with gefitinib or afatinib
398 monotherapy for 4 days, the mice treated with saline with 0.5% polyoxyethylene
399 sorbitan monooleate as vehicle, gefitinib monotherapy, FTY720 monotherpay and the
400 combination of gefitinib and FTY720 for 7 days, the mice treated with gefitinib or
401 afatinib monotherapy for 14 days, or the mice treated with prior gefitinib treatment for
402 14 days followed by saline with 0.5% polyoxyethylene sorbitan monooleate as vehicle,
403 anti-PD-1, anti-VEGFR2 or the combination of anti-PD-1 and anti-VEGFR2 for 7 days.
404 Spleens were collected at day 3 from the mice treated with saline with 0.5%
405 polyoxyethylene sorbitan monooleate as vehicle.

406

407 **Flow cytometry (FCM) analysis**

408 Tumor tissues of syngeneic *Egfr*-mutant lung cancer mouse model were dissected from
409 the mice and dissociated into single-cell suspensions as described above, and red blood
410 cells were removed using a red blood cell lysis solution (Miltenyi Biotec, catalog no.
411 130-094-183). Cells, which included tumor-infiltrating lymphocytes (TILs) and tumor
412 cells, were stained with the above indicated fluorescence-labeled antibodies and
413 subjected to FCM analysis. Briefly, cells were washed with FACS staining buffer
414 consisting of 2 mM EDTA (Thermo Fisher Scientific, catalog no. 15575020) and 0.5%

CD8⁺ T cell-dependent response in *Egfr*-mutant lung cancer

415 (w/v) bovine serum albumin (Sigma-Aldrich, catalog no. 10735078001) in phosphate-
416 buffered saline (PBS, pure water containing 0.02% KCL (Sigma-Aldrich, catalog no.
417 24-3290), 0.8% NaCL (Sigma-Aldrich, catalog no. 28-2270-5), 0.115% Na₂HPO₄
418 (Sigma-Aldrich, catalog no. 28-3750-5), 0.02% KH₂PO₄ (Sigma-Aldrich, catalog no.
419 169-04245), and incubated with monoclonal antibodies against surface markers for 30
420 minutes at 4°C in the FACS staining buffer. Intracellular Foxp3 staining was also
421 performed using a Foxp3 staining buffer set (Thermo Fisher Scientific, catalog no. 00-
422 5523-00). Zombie Violet Fixable Viability Kit (BioLegend catalog no. 423113) was
423 used to assess live or dead status. The samples were acquired using a MACS Quant
424 flow cytometer (Miltenyi Biotec), and the data were analyzed using FlowJo software
425 (version 10, TreeStar, Ashland, OR, USA). Tumor tissues were collected at day 3 from
426 the mice treated with saline with 0.5% polyoxyethylene sorbitan monooleate as vehicle,
427 gefitinib monotherapy, anti-VEGFR2, the combination of gefitinib and anti-PD-1,
428 combination of gefitinib and anti-VEGFR2, combination of anti-PD-1 and anti-
429 VEGFR2. Tumor tissues were also harvested from the mice treated with gefitinib for 4
430 or 14 days.

431

432 **Cytokine arrays**

CD8⁺ T cell-dependent response in *Egfr*-mutant lung cancer

433 Tumor tissues treated with saline with with 0.5% polyoxyethylene sorbitan monooleate
434 as vehicle or gefitinib for 3 days were harvested and immediately frozen with screw cap
435 micro tubes (Sarstedt, Nümbrecht, Germany, catalog no. 72.694.007) in liquid nitrogen.
436 10 mg of the frozen tissues were measured by electronic scale (A&D Weighing, Tokyo,
437 Japan, HF-2000). The tissues were mixed with 500 µl PBS with 1% Triton-X (nacalai
438 tesque, catalog no. 35501-02) and mechanically homogenized using a homogenizer
439 (IKA, Staufen, Germany, catalog no. T10 basic ULTRA-TURRAX) with shaft
440 generator (IKA, Staufen, Germany, catalog no. S10N-5G). The lysate was centrifuged
441 for 30 minutes at 14,000 rpm at 4°C and the supernatant was used for cytokine array.
442 The Proteome Profiler Mouse Cytokine Array Kit, Panel A (R&D Systems,
443 Minneapolis, MN, USA, catalog no. ARY006) was used according to the
444 manufacturer's instructions. Briefly, the supernatant was mixed with 500µL of Buffer 4
445 and Buffer 6 was added to bring the total volume to 1.5mL.
446 15 µL of Detection Antibody Cocktail was added in the solution and incubated at room
447 temperature for an hour. Then, the membrane with pre-soaked in Array Buffer 6 for an
448 hour were incubate with the solution overnight at 4 °C. Dots were detected using an
449 ImageQuant LAS-4000 imager (GE Healthcare Biosciences, Chicago, IL, USA). The
450 mean pixel density was measured using the ImageJ software (version 1.52a).

451 Expression level of each cytokine was normalized using reference spots on the
452 membrane, then the relative expression levels were calculated between the samples.

453

454 **Statistical analysis**

455 Statistical analyses were performed using GraphPad Prism 9.1. (GraphPad Software,
456 San Diego, CA, USA). Two-sided Student's t-tests were used for comparison of the
457 means of data between two groups, and one-way ANOVA with post-hoc Tukey's test
458 was used for comparisons among multiple independent groups, unless otherwise
459 specified. The survival probability was calculated using the Kaplan–Meier method, and
460 differences in survival were evaluated using the Log-rank test with Bonferroni
461 correction. Statistical significance was set at $P < 0.05$.

462

463 **Data Availability**

464 The data generated in this study are available within the article and its supplementary
465 data files. RNA-seq data analyzed in this study are available in the NCBI Gene
466 Expression Omnibus (GEO) repository (GSE197260).

467

468 **Results**

469 **CD8⁺ T cell-dependent immunity in *Egfr*-mutant lung cancers.**

470 First, we assessed the impact of *Egfr* mutation on tumor immunity in the lungs. The
471 expression profiles of 750 immune-related genes were assessed between the lungs from
472 wild-type mice and those from the genetically engineered mice harboring *Egfr* exon 19
473 deletion using NanoString nCounter analysis (29)(Fig. 1A, left). Expectedly, *Egfr* was
474 upregulated 16-fold in the lungs of transgenic mice compared to wild-type mice. In
475 contrast, immune-related genes, including *Gzma* or *Ccl5*, were generally downregulated
476 in the lungs with *Egfr* mutation (Suppl. Fig. S1A-B, Suppl. Table S1). Genes related to
477 T-lymphocyte, natural killer (NK) cell, and B-lymphocyte function were significantly
478 decreased (Fig. 1A, right).

479 Next, we assessed the impact of EGFR inhibition on the TME in an *Egfr*-mutant
480 syngeneic lung cancer model. The EGFR-TKI gefitinib showed an inhibitory effect on
481 tumor growth in a dose-dependent manner (Suppl. Fig. S1C). The TME in mice treated
482 with gefitinib (50 mg/kg) for 3 days was then compared with control vehicle-treated
483 mice (Fig. 1B). Tumor volume was decreased, and cytokines related to CD8⁺ T cells,
484 such as MIP-1 α , MIP-1 β , MIG/CXCL9, RANTES/CCL5, and IP-10/CXCL10, were
485 increased in tumors treated with the EGFR inhibitor (Fig. 1C)(4,30,31). On the other
486 hand, cytokines related to regulatory T cells (Tregs), such as TARC/CCL17, were

487 decreased in tumors treated with EGFR inhibitors (Fig. 1C)(31). Consistently, IHC and
488 FCM analyses revealed a significant increase in the CD8⁺ T-cell/Treg ratio in the
489 tumors treated with gefitinib (vehicle: 0.46±0.03 vs. gefitinib: 1.08±0.11,
490 mean±SE)(Fig. 1D-E, Suppl. Fig. S1D-E). We also analyzed the expression of MHC
491 class I in the tumor cells. We found that the expression of H-2Kb and H-2Db were
492 increased in *Egfr*-mutant lung cancer cells treated with the EGFR-TKI (Suppl. Fig.
493 S2A-B), suggesting IFN involvement.

494 We next examined the impact of CD8⁺ T-cell depletion on tumor growth in our
495 mouse model. Tumor-bearing mice were treated with gefitinib for 2 weeks and
496 subsequently observed for 2 weeks with or without CD8⁺ T-cell depletion. Gefitinib
497 reduced the tumor volume to the same extent in mice with or without CD8⁺ T-cell
498 depletion. However, tumor regrowth was observed earlier in mice administered anti-
499 CD8 than in mice treated with the isotype control (Fig. 1F). In contrast, depletion of
500 CD8⁺ T cells had little effect on tumor growth in mice without gefitinib treatment (Fig.
501 1G). We also assessed the effect of FTY720 (analog of sphingosine 1-phosphate),
502 which inhibits lymphocyte infiltration into tumors (32). FTY720 monotherapy had little
503 impact on the number of CD8⁺ T cells in the TME and exerted little inhibitory effect on
504 tumor growth in *Egfr*-mutated tumors (Suppl. Fig. S2CD). In contrast, the number of

505 CD8⁺ T cells was significantly reduced and earlier regrowth was observed in mice
506 treated with gefitinib and FTY720 than in those treated with gefitinib alone (Suppl. Fig.
507 S2C, S2E), suggesting that the increase in CD8⁺ T-cell number in tumors was mainly
508 due to the cells that migrated from outside the tumor area. These findings suggest that
509 oncogenic EGFR signaling influences the immunosuppressive TME and that CD8⁺ T
510 cell-dependent tumor immunity was responsible for the inhibitory effect of EGFR-TKIs
511 on tumor growth in *Egfr*-mutant lung cancer.

512

513 **The effect of anti-PD-1 inhibitor in *Egfr*-mutant lung cancer.**

514 Next, we investigated PD-1 and ligand expression in our syngeneic mouse model.
515 First, PD-1 expression, which is thought to be a key co-inhibitory receptor in the
516 process of T-cell activation and exhaustion (33,34), on CD8⁺ T cells in the TME was
517 assessed. The number of PD-1⁺CD8⁺ T cells tended to increase, but the difference was
518 not statistically significant (Fig. 2A). We also assessed the expression of PD-1 ligands,
519 PD-L1 and PD-L2, on cancer cells. Neither PD-L1 nor PD-L2 was detected on lung
520 cancer cells harboring the *Egfr* mutation after gefitinib exposure (Fig. 2B), and neither
521 stimulation with IFN γ nor IFN α increased the expression of these inhibitory molecules
522 on the *Egfr*-mutant lung cancer cells. However, the expression of PD-L1 was increased

523 in MC-38 mouse colon cancer cells, which expressed PD-L1 or PD-L2 at baseline, and
524 PD-L2 expression was maintained with IFN γ or IFN α stimulation (Fig. 2C)(35).
525 We then tested the inhibitory effect of PD-1 inhibition on tumor growth. Consistent
526 with a previous report (35), anti-PD-1 significantly inhibited tumor growth in a
527 syngeneic mouse model derived from MC-38 cells in C57BL/6J mice (Suppl. Fig. S3);
528 however, it showed little inhibitory effect on tumor growth in the *Egfr*-mutant
529 syngeneic model (Fig. 2D). The number of CD8⁺ T cells and Tregs showed a small
530 significant increase, but the CD8⁺ T-cell/Treg ratio was not increased in tumors treated
531 with anti-PD-1 alone compared with to tumors treated with the isotype control (Fig.
532 2E). We also tested the concomitant combination gefitinib and anti-PD-1 on tumor
533 growth in the *Egfr*-mutant tumors. Consistent with a previous report (36), no additional
534 significant tumor growth inhibition was achieved by the combination therapy (Fig. 2F),
535 and the combination also had little impact on CD8⁺ T cells and Tregs in the TME
536 compared to gefitinib alone (Fig. 2G).

537

538 **The effect of anti-VEGFR2 in *Egfr*-mutant lung cancer.**

539 We next investigated the effect of anti-VEGFR2, which is clinically approved
540 for the treatment of *EGFR*-mutant lung cancer (17). IHC showed that the expression of

541 CD31, an angiogenic marker, was decreased in *Egfr*-mutant tumors 3 days after the
542 initiation of anti-VEGFR2 (Fig 3A). It has been reported that Fas ligand (FasL) on the
543 tumor vascular endothelium is involved in the elimination to CD8⁺ T cells and the
544 recruitment of Tregs (37); therefore, we also assessed the localization of FasL
545 expression. IHC analysis revealed that the expression of FasL and VEGFR2 proteins
546 were mainly increased on tumor cells from mice treated with gefitinib (Suppl. Fig.
547 S4A)(38,39). Anti-VEGFR2 alone showed a small, but significant, inhibitory effect on
548 tumor growth (Fig. 3B) and did not increase the number of CD8⁺ T cells, but Tregs
549 were increased in the TME compared to tumors treated with the isotype control,
550 resulting in a decrease in the CD8⁺ T-cell/Treg ratio 3 days after the administration of
551 anti-VEGFR2 (Fig. 3C-E). We then assessed the inhibitory effect of combination
552 therapy with gefitinib and anti-VEGFR2 on tumor growth in *Egfr*-mutant lung cancer.
553 The mice were treated with gefitinib alone or in combination with anti-VEGFR2 for 2
554 weeks and subsequently observed for 2 weeks. The inhibitory effect on tumor growth
555 was similar between the mice treated with the gefitinib alone and those that received the
556 combination therapy (Suppl. Fig. S4B), and neither combination nor monotherapy
557 sustained the tumor inhibitory effect (Fig. 3F). The number of CD8⁺ T cells in the TME
558 was significantly increased in the tumors of mice treated with the combination of

559 gefitinib and anti-VEGFR2 compared with the mice treated with gefitinib alone (Fig.
560 3C, 3G). However, the number of Tregs was also increased in these tumors, resulting in
561 no effect on CD8⁺ T-cell/Treg ratio in tumors with the combination therapy compared
562 with alone (Fig. 3D, 3G).

563

564 **The effect of dual blockade of PD-1/VEGFR in *Egfr* mutant lung cancer.**

565 Concomitant combination of EGFR-TKI plus PD-1 inhibition or EGFR-TKI plus
566 VEGFR2 inhibition did not induce a sustained inhibitory effect in the *Egfr*-mutant lung
567 cancer. Therefore, we performed RNA-seq on tumors treated with or without EGFR-
568 TKI. Consistent with the cytokine array (Fig. 1C), RNA-seq showed increased
569 expression of *Cxcl9* and *Cxcl10/Cxcr3*, and decreased expression of *Ccl17* in tumors
570 treated with EGFR-TKI (Suppl. Fig. S5A-B). The expression of immunosuppressive
571 chemokines and chemokine receptors were also increased, such as *Tgfb1*, *Cxcr4*, *Ccr2*,
572 and *Ccr5* (Suppl. Fig. S5C), which are reported to suppress cytotoxic T-cell functions or
573 are related to resistance to anti-PD-1 or anti-VEGFR2 (40,41). Previous studies suggest
574 that these genes are involved in the recruitment and the activation of tumor-associated
575 macrophages (42). Consistently the number of CD206⁺ M2-like macrophages was
576 increased in tumors treated with EGFR-TKI (Suppl. Fig. S6A-B). The expression of

577 these chemokines and chemokines receptors, as well as the number of CD206⁺ cells via
578 IHC, reverted after the discontinuation of EGFR-TKI (Suppl. Fig. S5C, Suppl. Fig.
579 S6C-D), suggesting that these cell types correlated with the inhibition of oncogenic
580 EGFR signaling.

581 We next assessed the effect of dual PD-1/VEGFR2 blockade in tumors without
582 EGFR inhibition, which has shown promising results in clinical trials for NSCLC (21).
583 However, the anti-PD-1/anti-VEGFR2 combination therapy showed no superior
584 inhibitory effect on tumor growth compared to anti-PD-1 alone in the *Egfr*-mutant lung
585 cancer model (without EGFR inhibition)(Fig. 4A). The combination also did not
586 significantly change the number of CD8⁺ T cells or Tregs nor the CD8⁺ T-cell/Treg
587 ratio in the TME compared to anti-PD-1 alone in the *Egfr*-mutant lung cancer model
588 (Fig. 4B).

589

590 **Impact of pretreatment with EGFR-TKI for sequential PD-1/VEGFR2 inhibition.**

591 Last, based on these results, we assessed the effect of dual PD-1/VEGFR2 blockade
592 in *Egfr*-mutated lung cancer pre-treated with EGFR-TKI. Because the increase in the
593 CD8⁺ T-cell/Treg ratio was relatively low in tumors treated with gefitinib for 3 days, we
594 assessed the ratio on day 14 after gefitinib initiation, when tumor reduction was

595 maximized. As a result, the CD8⁺ T-cell/Treg ratio was significantly increased (Fig. 5A-
596 B), and PD-1⁺CD8⁺ T cells in tumors of mice treated with gefitinib for 14 days was also
597 increased compared with that in the tumors treated for 3 days (Fig. 5C), suggesting that
598 tumor-reactive CD8⁺ T cells were clonally expanded (33,43). CD107a (a marker for
599 degranulation) was also increased on CD8⁺ T cells after 14 days of treatment (Suppl.
600 Fig. S7A) (44).

601 We then assessed the effect of sequential administration of anti-PD-1, anti-VEGFR2,
602 or combination anti-PD-1/anti-VEGFR2 for 7 days in tumors pre-treated with gefitinib
603 for 14 days (Fig. 5D). As a result, sequential monotherapy with anti-PD-1 or anti-
604 VEGFR2 showed a small and non-significant inhibitory effects, and most tumors
605 regrew during the 2-week observation period (Fig. 5E). In contrast, the combination of
606 the anti-PD-1 and anti-VEGFR2 resulted in sustained tumor inhibition during the
607 observation period (Fig. 5E, 5F). No body weight loss was observed in the mice treated
608 with combination therapy (Suppl. Fig. S7B). To assess whether the treatment schedule
609 had an impact on the effect of dual blockade with anti-PD-1/anti-VEGFR2, we also
610 evaluated the effect of concomitant triple therapy with EGFR-TKI (gefitinib), anti-PD-
611 1, and anti-VEGFR2 on tumor growth in *Egfr*-mutant lung cancer. Tumor-bearing mice
612 were treated for 2 weeks, followed by a 2-week observation period (Suppl. Fig. S7C).

613 We performed this *in vivo* experiment three times; however, the concomitant triple
614 therapy exerted a smaller but significant inhibitory effect on tumor growth compared
615 with sequential triple therapy, and the sustained tumor inhibition was not reproduced in
616 the syngeneic *Egfr* mutant lung cancer model, suggesting that the treatment schedule
617 affected dual PD-1/VEGFR2 blockade efficacy (Suppl. Fig. S7D). The late concomitant
618 triple therapy was also tested, in which mice received prior EGFR-TKI monotherapy
619 for 2 weeks followed by the addition of combination of anti-PD-1 and anti-VEGFR2
620 with continuation of EGFR-TKI for a week. This regimen still it did not induce a
621 sustained tumor-inhibitory effect (Suppl. Fig. S8A-B), suggesting that the
622 discontinuation of EGFR inhibition may be crucial for inducing sustained tumor
623 immunity by dual PD-1/VEGFR2 blockade in *Egfr*-mutated lung cancer.

624 To determine whether CD8⁺ T cell-dependent tumor immunity contributed to tumor
625 inhibition, we examined the impact of CD8⁺ T-cell depletion in tumors treated with the
626 gefitinib, followed by sequential combination therapy with anti-PD-1 and anti-
627 VEGFR2. As expected, the tumors from mice treated with anti-CD8 rapidly regrew
628 compared with mice not given with the depleting antibody (Fig. 5G, 5H). These data
629 suggest that the inhibitory effect of the triple therapy (EGFR-TKI followed by the

630 sequential combination of anti-PD-1/anti-VEGFR2) on tumor growth is induced by

631 CD8⁺ T cell-dependent tumor immunity.

632 Finally, we assessed the TME in a *Egfr*-mutant lung cancer model treated with
633 gefitinib for 2 weeks, followed by sequential therapies for a week. Consistent with the
634 inhibitory effect on tumor growth, the highest number of CD8⁺ T cells was maintained
635 in tumors treated with combination anti-PD-1/anti-VEGFR2, whereas the number of
636 CD8⁺ T cells was decreased in tumors treated with each of the monotherapies or the
637 vehicle (Fig. 6A, 6B). CD11c⁺ dendritic cells (DCs) were also increased in the tumors
638 treated with combination anti-PD-1/anti-VEGFR2 among all groups (Fig. 6C, 6D).
639 Consistently, the expression of chemokines associated with T-cell activation, such as
640 *Ccl19* (45), was mostly increased in the tumors treated with the sequential dual PD-
641 1/VEGFR2 blockade (Fig. 6E), whereas the immunosuppressive chemokines and
642 receptors, such as *Tgfb1*, *Cxcr4*, *Ccr2* or *Ccr5*, were relatively maintained at lower
643 expression (Suppl. Fig. S5C). We also performed quanTIseq analysis to estimate the
644 type of TILs using the RNA-seq data (26). The fraction of NK cells or B lymphocytes
645 showed a similar trend with that of the CD8⁺ T cells or DCs (Suppl. Fig. S8C). In
646 contrast, the number of Tregs or CD206⁺ cells continued to be maintained at low
647 numbers in all tumors following each therapy (Fig. 6F, 6G Suppl. Fig. S6C-D).

648 Consequently, these changes in the TME might be involved in sustained tumor
649 inhibition induced by prior EGFR-TKI treatment followed by a combination of anti-PD-
650 1 and anti-VEGFR2 in lung cancer harboring *Egfr* mutation.

651

652 **Discussion**

653 A therapeutic strategy for activating CD8⁺ T cells has not been fully established for
654 lung cancer with non-smoking-related oncogenes and non-inflamed TMEs. To the best
655 of our knowledge, this is the first report demonstrating that CD8⁺ T cell-dependent
656 tumor immunity is responsible for the tumor inhibitory effect of EGFR-TKIs in lung
657 cancer harboring *Egfr* mutation *in vivo*. We also found that the treatment schedule and
658 TME status were critical for the efficacy of dual blockade against PD-1 and VEGFR2 in
659 *Egfr*-mutant lung cancer. Prior EGFR-TKI treatment increased the CD8⁺ T-cell/Treg
660 ratio, and sequential combination therapy with anti-PD-1 and anti-VEGFR2 sustained
661 CD8⁺ T-cell anti-tumor immunity, although the dual PD-1/VEGFR2 blockade, itself,
662 had a minor inhibitory effect on tumor growth in *Egfr*-mutant lung cancer without
663 EGFR-TKI pre-treatment. Concomitant triple therapy with EGFR-TKI, anti-PD-1, and
664 anti-VEGFR2 failed to induce sustained tumor inhibition. The data showed that
665 combination EGFR-TKI and anti-VEGFR2 increased the number of Tregs and did not

666 increase the CD8⁺ T-cell/Treg ratio in the TME at an early phase)—this might explain
667 the unexpected result. This study also revealed that the expression of
668 immunosuppressive factors, such as *Tgfb1*, *Cxcr4*, or the number of M2-like
669 macrophages, were increased with the initiation of EGFR-TKI, and the discontinuation
670 of EGFR-TKI reversed the transient increase in these factors. Thus, the combination of
671 anti-PD-1 and anti-VEGFR2 might be less affected by immunosuppressive factors in
672 the sequential than in the concomitant setting. In addition to the CD8⁺ T-cell/Treg
673 balance, the fluctuation in the levels of these immunosuppressive factors might be
674 another explanation why the sequential administration of PD-1 and VEGFR2 inhibitors
675 was effective. Further validation may be needed to establish an ideal treatment schedule
676 for clinical application. However, we believe that the findings in this study may pave
677 the way for a novel immunotherapy strategy for lung cancer harboring *EGFR* mutations.

678 We previously reported that our lung cancer model reflects the clinical course of
679 EGFR-TKI treatment in human lung cancer harboring *EGFR* mutations (24). In this
680 study, we also confirmed that our model partially reproduced the clinical course of ICI
681 treatment in lung cancer harboring *Egfr* mutations. Our *Egfr*-mutant lung cancer model
682 was derived from type 2 pneumocytes with low expression of PD-L1, and PD-1
683 inhibition or concomitant combination therapy with EGFR-TKI and anti-PD-1 had

684 limited effect on tumor growth, which reflects the clinical observation of human lung
685 cancer harboring *EGFR* mutations (46). Sugiyama et al. reveals that EGFR signaling in
686 cancer cells plays an important role in creating the non-inflamed TME of lung cancer
687 harboring EGFR mutations (4). They also showed that the CD8⁺ T-cell/Treg ratio was
688 increased in clinical samples treated with EGFR-TKIs. Our mouse model had a non-
689 inflamed TME, in which a small number of CD8⁺ T cells existed, but EGFR-TKI
690 administration increased CD8⁺ T cells compared to Tregs, recapitulating their analysis
691 using clinical samples. Akbay et al. also report the effect of anti-PD-1 using a
692 genetically engineered lung cancer mouse model harboring a human *EGFR* mutations
693 that is driven by the CCSP promoter, which targets Clara cells (47), and has high PD-
694 L1 expression. Anti-PD-1 antibody alone in this setting effectively inhibits *EGFR*-
695 mutant lung cancer, but this model does not reflect the typical human lung cancer
696 harboring *EGFR* mutations. Consequently, we believe that our syngeneic lung cancer
697 mouse model is unique and more accurately reflects the tumor immune response of
698 human lung cancer harboring *EGFR* mutations.

699 Our study suggests that the effect of the dual blockade of PD-1 and VEGFR2 was
700 restricted by the TME status and that pre-treatment with EGFR-TKI was required to
701 modify the TME in lung cancer harboring *EGFR* mutations. In addition to the

702 expression of PD-1 on CD8⁺ T cells (34) or the expression of the CXCL9/CXCR3 axis
703 in the TME (48), another study reveals that the PD-1⁺CD8⁺ T-cell/Treg ratio is
704 important for predicting the positive effect of ICIs in NSCLC (43). Currently, multiple
705 clinical studies investigating the combination of ICIs and anti-angiogenic agents in
706 order to accelerate tumor immunity have been conducted (16); however, the CD8⁺ T-
707 cell/Treg balance might still be an important predictive factor for the effect of dual
708 blockade of PD-L1/PD-1 and VEGF/VEGFR2 pathways, suggesting that the pre-
709 treatment is required for cancers with a low CD8⁺ T-cell/Treg ratio. Tu et al. reveals
710 that the second-generation EGFR-TKI, afatinib, with a relatively high ability to inhibit
711 wild-type EGFR, suppresses the proliferation of CD8⁺ T cells by targeting pyrimidine
712 biosynthesis at an early time point and shows the beneficial effect of sequential therapy
713 with afatinib followed by anti-PD-1 in an EGFR-wild-type lung cancer model (49). The
714 direct effect of EGFR-TKI on stromal immune cells might also be explanation why the
715 sequential treatment was effective.

716 However, these findings raise the question of why not only PD-1 inhibition, but
717 also VEGFR blockade, is required as a sequential therapy to sustain tumor inhibition in
718 the *EGFR*-mutant lung cancer model. The TME is composed of a complex balance of
719 multiple types of immunostimulatory and suppressive factors (50). Several studies

720 indicate that anti-angiogenic agents have a positive effect on tumor immunity by
721 inhibiting immunosuppressive cells, including Tregs, but our findings suggest that
722 VEGFR2 inhibition has a limited effect on inhibiting Tregs. Anti-VEGFR might inhibit
723 other suppressive immune cells in addition to Tregs. We also found that the expression
724 of FasL and VEGFR2 was increased on *Egfr*-mutated tumor cells treated with EGFR-
725 TKI. A previous study suggests that expression of FasL on cancer cells is involved in
726 the suppression of cytotoxic T lymphocytes (39), and we previously reported that anti-
727 VEGFR2 can directly inhibit *EGFR*-mutated lung cancer cells expressing VEGFR2
728 (38). Consequently, PD-1 inhibition may activate CD8⁺ T cells, and anti-VEGFR2
729 might further enhance activation of CD8⁺ T cells through inhibiting suppressive
730 immune cells or cancer cells expressing VEGFR2 and FasL in the sequential
731 administration setting.

732 Our study has several limitations. First, we did not verify our findings in human lung
733 cancer samples. Second, we did not verify our findings in other types of *EGFR* mutant
734 cancers, although its known that the type of mutations or co-occurring mutations can
735 affect the efficiency of ICIs (51,52). Third, we assessed only a subset of immune cells
736 (CD8⁺ T cells and Tregs) but did not comprehensively evaluate the role of other
737 immune cells or stromal cells in the TME. Considering the complex interaction of the

738 immune network, dual blockade of PD-1 and VEGFR2 could affect multiple immune
739 cells or stromal cells. Single-cell analysis may provide further details on the type of
740 immune cells or stromal cells that are targeted by PD-1 and VEGFR2 inhibitors or
741 provide insight into the complex interactions of immune cells leading to CD8⁺ T-cell
742 activation. However, our lung cancer model more accurately reproduced the clinical
743 features of lung cancer compared to existing models to certain extent; thus, the findings
744 of this study may have potential implications to develop an alternative treatment
745 strategy for human lung cancer harboring *EGFR* mutations.

746 In conclusion, we demonstrated that *EGFR*-mutated lung cancer with a non-inflamed
747 TME could be suppressed by combined immunotherapy. CD8⁺ T cell-dominant TME
748 induced by EGFR inhibition and the discontinuation of EGFR-TKI, which reverted the
749 transient increase of immunosuppressive factors, may be an important factor defining
750 the effect and treatment schedule of combination therapy with anti-PD-1 and anti-
751 VEGFR2. This study provides new insights into the potential for combined
752 immunotherapy strategies for malignant diseases with expression of driver oncogenes
753 and a non-inflamed TME.

754

755 **Acknowledgements**

756 We are grateful to Ms. Hiromi Nakashima, Ms. Kyoko Maeda from Department of
757 Hematology, Oncology and Respiratory Medicine, Okayama University Graduate
758 School of Medicine, Dentistry and Pharmaceutical Sciences, and Dr. Takehiro
759 Matsubara, Okayama University Hospital Biobank, Okayama University Hospital for
760 the technical support. We also thank our laboratory colleagues for the useful
761 discussions.

762

763 REFERENCES

- 764 1. Chamoto K, Hatae R, Honjo T. Current issues and perspectives in PD-1
765 blockade cancer immunotherapy. *Int J Clin Oncol.* 2020;25:790-800.
- 766 2. Gainor JF, Shaw AT, Sequist LV, Fu X, Azzoli CG, Piotrowska Z, et al. EGFR
767 Mutations and ALK Rearrangements Are Associated with Low Response Rates
768 to PD-1 Pathway Blockade in Non-Small Cell Lung Cancer: A Retrospective
769 Analysis. *Clinical cancer research : an official journal of the American*
770 *Association for Cancer Research.* 2016;22:4585-93.
- 771 3. Lee CK, Man J, Lord S, Links M, GebSKI V, Mok T, et al. Checkpoint Inhibitors in
772 Metastatic EGFR-Mutated Non-Small Cell Lung Cancer—A Meta-Analysis.
773 *Journal of Thoracic Oncology.* 2017;12:403-7.
- 774 4. Sugiyama E, Togashi Y, Takeuchi Y, Shinya S, Tada Y, Kataoka K, et al.
775 Blockade of EGFR improves responsiveness to PD-1 blockade in EGFR-
776 mutated non-small cell lung cancer. *Sci Immunol.* 2020; 5(43):eaav3937.
- 777 5. Saito M, Shiraishi K, Kunitoh H, Takenoshita S, Yokota J, Kohno T. Gene
778 aberrations for precision medicine against lung adenocarcinoma. *Cancer Sci.*
779 2016;107:713-20.
- 780 6. Nishii K, Ohashi K, Tamura T, Ninomiya K, Matsubara T, Senoo S, et al.
781 Detection of epidermal growth factor receptor mutations in exhaled breath
782 condensate using droplet digital polymerase chain reaction. *Oncol Lett.* 2020;
783 20(6):393
- 784 7. Ohashi K, Maruvka YE, Michor F, Pao W. Epidermal growth factor receptor
785 tyrosine kinase inhibitor-resistant disease. *J Clin Oncol.* 2013;31:1070-80.

- 786 8. Ninomiya K, Ohashi K, Makimoto G, Tomida S, Higo H, Kayatani H, et al. MET or
787 NRAS amplification is an acquired resistance mechanism to the third-
788 generation EGFR inhibitor naquotinib. *Sci Rep.* 2018;8:1955.
- 789 9. Ohashi K, Ninomiya K, Yoshioka H, Bessho A, Shibayama T, Aoe K, et al. Impact
790 of HER2 expression on EGFR-TKI treatment outcomes in lung tumors harboring
791 EGFR mutations: A HER2-CS study subset analysis. *Lung Cancer.* 2020;150:83-
792 9.
- 793 10. Kayatani H, Ohashi K, Ninomiya K, Makimoto G, Nishii K, Higo H, et al. Beneficial
794 effect of erlotinib and trastuzumab emtansine combination in lung tumors
795 harboring EGFR mutations. *Biochem Biophys Res Commun.* 2020;532:341-6.
- 796 11. Calles A, Riess JW, Brahmer JR. Checkpoint Blockade in Lung Cancer With
797 Driver Mutation: Choose the Road Wisely. *Am Soc Clin Oncol Educ Book.*
798 2020;40:372-84.
- 799 12. Creelan BC, Yeh TC, Kim S-W, Nogami N, Kim D-W, Chow LQM, et al. A Phase
800 1 study of gefitinib combined with durvalumab in EGFR TKI-naive patients with
801 EGFR mutation-positive locally advanced/metastatic non-small-cell lung
802 cancer. *British Journal of Cancer.* 2021; 124(2):383-390.
- 803 13. Oxnard GR, Yang JC-H, Yu H, Kim S-W, Saka H, Horn L, et al. TATTON: a
804 multi-arm, phase Ib trial of osimertinib combined with selumetinib, savolitinib, or
805 durvalumab in EGFR-mutant lung cancer. *Annals of Oncology.* 2020;31(4):507-
806 16.
- 807 14. Chalmers AW, Patel S, Boucher K, Cannon L, Esplin M, Luckart J, et al. Phase I
808 Trial of Targeted EGFR or ALK Therapy with Ipilimumab in Metastatic NSCLC
809 with Long-Term Follow-Up. *Target Oncol.* 2019;14:417-21.
- 810 15. Riudavets M, Naigeon M, Texier M, Dorta M, Barlesi F, Mazieres J, et al.
811 Gefitinib plus tremelimumab combination in refractory non-small cell lung
812 cancer patients harbouring EGFR mutations: The GEFTREM phase I trial. *Lung*
813 *Cancer.* 2021;S0169-5002(21)00624-3.
- 814 16. Yi M, Jiao D, Qin S, Chu Q, Wu K, Li A. Synergistic effect of immune checkpoint
815 blockade and anti-angiogenesis in cancer treatment. *Molecular Cancer.* 2019;18
816 (1):60.

- 817 17. Ninomiya K, Teraoka S, Zenke Y, Kenmotsu H, Nakamura Y, Okuma Y, et al.
818 Japanese Lung Cancer Society Guidelines for Stage IV NSCLC With EGFR
819 Mutations. *JTO Clin Res Rep.* 2021;2:100107.
- 820 18. Zhou Q, Xu C-R, Cheng Y, Liu Y-P, Chen G-Y, Cui J-W, et al. Bevacizumab
821 plus erlotinib in Chinese patients with untreated, EGFR-mutated, advanced
822 NSCLC (ARTEMIS-CTONG1509): A multicenter phase 3 study. *Cancer Cell.*
823 2021;39:1279–1291.e3.
- 824 19. Finn RS, Qin S, Ikeda M, Galle PR, Ducreux M, Kim T-Y, et al. Atezolizumab
825 plus Bevacizumab in Unresectable Hepatocellular Carcinoma. *New England*
826 *Journal of Medicine.* Massachusetts Medical Society; 2020;382:1894–905.
- 827 20. Socinski MA, Jotte RM, Cappuzzo F, Orlandi F, Stroyakovskiy D, Nogami N, et
828 al. Atezolizumab for First-Line Treatment of Metastatic Nonsquamous NSCLC.
829 *New England Journal of Medicine.* Massachusetts Medical Society;
830 2018;378:2288–301.
- 831 21. Herbst RS, Arkenau H-T, Santana-Davila R, Calvo E, Paz-Ares L, Cassier PA,
832 et al. Ramucirumab plus pembrolizumab in patients with previously treated
833 advanced non-small-cell lung cancer, gastro-oesophageal cancer, or urothelial
834 carcinomas (JVDF): a multicohort, non-randomised, open-label, phase 1a/b
835 trial. *The Lancet Oncology.* Elsevier; 2019;20:1109–23.
- 836 22. Ohashi K, Rai K, Fujiwara Y, Osawa M, Hirano S, Takata K, et al. Induction of
837 lung adenocarcinoma in transgenic mice expressing activated EGFR driven by
838 the SP-C promoter. *Cancer Sci.* 2008;99:1747–53.
- 839 23. Ohashi K, Takigawa N, Osawa M, Ichihara E, Takeda H, Kubo T, et al.
840 Chemopreventive effects of gefitinib on nonsmoking-related lung tumorigenesis
841 in activating epidermal growth factor receptor transgenic mice. *Cancer Res.*
842 2009;69:7088–95.
- 843 24. Higo H, Ohashi K, Makimoto G, Nishii K, Kudo K, Kayatani H, et al. EGFR-TKI
844 acquired resistance in lung cancers harboring EGFR mutations in
845 immunocompetent C57BL/6J mice. *Lung Cancer.* Elsevier; 2019;136:86–93.
- 846 25. Li T, Fu J, Zeng Z, Cohen D, Li J, Chen Q, et al. TIMER2.0 for analysis of
847 tumor-infiltrating immune cells. *Nucleic Acids Res.* 2020;48:W509–14.

- 848 26. Finotello F, Mayer C, Plattner C, Laschober G, Rieder D, Hackl H, et al.
849 Molecular and pharmacological modulators of the tumor immune contexture
850 revealed by deconvolution of RNA-seq data. *Genome Medicine*. 2019;11:34.
- 851 27. Kudo K, Ohashi K, Makimoto G, Higo H, Kato Y, Kayatani H, et al. Triplet
852 therapy with afatinib, cetuximab, and bevacizumab induces deep remission in
853 lung cancer cells harboring EGFR T790M in vivo. *Mol Oncol*. 2017;11:670–81.
- 854 28. Makimoto G, Ohashi K, Tomida S, Nishii K, Matsubara T, Kayatani H, et al. Rapid
855 Acquisition of Alectinib Resistance in ALK-Positive Lung Cancer With High
856 Tumor Mutation Burden. *J Thorac Oncol*. 2019;14:2009–18.
- 857 29. Cesano A. nCounter® PanCancer Immune Profiling Panel (NanoString
858 Technologies, Inc., Seattle, WA). *J Immunother Cancer*. 2015;3:42.
- 859 30. Taub DD, Conlon K, Lloyd AR, Oppenheim JJ, Kelvin DJ. Preferential migration
860 of activated CD4⁺ and CD8⁺ T cells in response to MIP-1 alpha and MIP-1
861 beta. *Science*. 1993;260:355–8.
- 862 31. Kohli K, Pillarisetty VG, Kim TS. Key chemokines direct migration of immune
863 cells in solid tumors. *Cancer Gene Ther*. Nature Publishing Group; 2022;29:10–
864 21.
- 865 32. Tang H, Wang Y, Chlewicki LK, Zhang Y, Guo J, Liang W, et al. Facilitating T Cell
866 Infiltration in Tumor Microenvironment Overcomes Resistance to PD-L1
867 Blockade. *Cancer Cell*. 2016;29:285–96.
- 868 33. Gros A, Robbins PF, Yao X, Li YF, Turcotte S, Tran E, et al. PD-1 identifies the
869 patient-specific CD8⁺ tumor-reactive repertoire infiltrating human tumors. *J
870 Clin Invest*. 2014;124:2246–59.
- 871 34. Thommen DS, Koelzer VH, Herzig P, Roller A, Trefny M, Dimeloe S, et al. A
872 transcriptionally and functionally distinct PD-1⁺ CD8⁺ T cell pool with
873 predictive potential in non-small-cell lung cancer treated with PD-1 blockade.
874 *Nat Med*. Nature Publishing Group; 2018;24:994–1004.
- 875 35. Terawaki S, Chikuma S, Shibayama S, Hayashi T, Yoshida T, Okazaki T, et al.
876 IFN- α Directly Promotes Programmed Cell Death-1 Transcription and Limits
877 the Duration of T Cell-Mediated Immunity. *JCI*. 2011;186:2772–9.

- 878 36. Brägelmann J, Lorenz C, Borchmann S, Nishii K, Wegner J, Meder L, et al.
879 MAPK-pathway inhibition mediates inflammatory reprogramming and sensitizes
880 tumors to targeted activation of innate immunity sensor RIG-I. *Nat*
881 *Commun.*2021;12 (1):5505.
- 882 37. Motz GT, Santoro SP, Wang L-P, Garrabrant T, Lastra RR, Hagemann IS, et al.
883 Tumor endothelium FasL establishes a selective immune barrier promoting
884 tolerance in tumors. *Nat Med.* 2014;20:607-15.
- 885 38. Watanabe H, Ichihara E, Kayatani H, Makimoto G, Ninomiya K, Nishii K, et al.
886 VEGFR2 blockade augments the effects of tyrosine kinase inhibitors by
887 inhibiting angiogenesis and oncogenic signaling in oncogene-driven non-small-
888 cell lung cancers. *Cancer Sci.* 2021;112:1853-64.
- 889 39. Ryan AE, Shanahan F, O'Connell J, Houston AM. Addressing the "Fas
890 Counterattack" Controversy: Blocking Fas Ligand Expression Suppresses
891 Tumor Immune Evasion of Colon Cancer *In vivo.* *Cancer Res.* 2005;65:9817-23.
- 892 40. Thomas DA, Massagué J. TGF- β directly targets cytotoxic T cell functions
893 during tumor evasion of immune surveillance. *Cancer Cell.* 2005;8:369-80.
- 894 41. Jung K, Heishi T, Incio J, Huang Y, Beech EY, Pinter M, et al. Targeting
895 CXCR4-dependent immunosuppressive Ly6Clow monocytes improves
896 antiangiogenic therapy in colorectal cancer. *Proc Natl Acad Sci U S A.*
897 2017;114:10455-60.
- 898 42. Mantovani A, Marchesi F, Malesci A, Laghi L, Allavena P. Tumour-associated
899 macrophages as treatment targets in oncology. *Nat Rev Clin Oncol.*
900 2017;14:399-416.
- 901 43. Kumagai S, Togashi Y, Kamada T, Sugiyama E, Nishinakamura H, Takeuchi Y, et
902 al. The PD-1 expression balance between effector and regulatory T cells
903 predicts the clinical efficacy of PD-1 blockade therapies. *Nat Immunol.*
904 2020;21:1346-58.
- 905 44. Aktas E, Kucuksezer UC, Bilgic S, Erten G, Deniz G. Relationship between
906 CD107a expression and cytotoxic activity. *Cell Immunol.* 2009;254:149-54.

- 907 45. Adachi K, Kano Y, Nagai T, Okuyama N, Sakoda Y, Tamada K. IL-7 and CCL19
908 expression in CAR-T cells improves immune cell infiltration and CAR-T cell
909 survival in the tumor. *Nat Biotechnol.* 2018;36:346-51.
- 910 46. Qiao M, Jiang T, Liu X, Mao S, Zhou F, Li X, et al. Immune Checkpoint Inhibitors
911 in EGFR-Mutated NSCLC: Dusk or Dawn? *J Thorac Oncol.* 2021;S1556-
912 0864(21)02113-4.
- 913 47. Akbay EA, Koyama S, Carretero J, Altabef A, Tchaicha JH, Christensen CL, et
914 al. Activation of the PD-1 pathway contributes to immune escape in EGFR-
915 driven lung tumors. *Cancer Discov.* 2013;3:1355-63.
- 916 48. Chow MT, Ozga AJ, Servis RL, Frederick DT, Lo JA, Fisher DE, et al.
917 Intratumoral Activity of the CXCR3 Chemokine System Is Required for the
918 Efficacy of Anti-PD-1 Therapy. *Immunity.* 2019;50:1498-1512.e5.
- 919 49. Tu H-F, Ko C-J, Lee C-T, Lee C-F, Lan S-W, Lin H-H, et al. Afatinib Exerts
920 Immunomodulatory Effects by Targeting the Pyrimidine Biosynthesis Enzyme
921 CAD. *Cancer Res.* 2021;81:3270-82.
- 922 50. Galli F, Aguilera JV, Palermo B, Markovic SN, Nisticò P, Signore A. Relevance
923 of immune cell and tumor microenvironment imaging in the new era of
924 immunotherapy. *Journal of Experimental & Clinical Cancer Research.*
925 2020;39:89.
- 926 51. Hastings K, Yu HA, Wei W, Sanchez-Vega F, DeVeaux M, Choi J, et al. EGFR
927 mutation subtypes and response to immune checkpoint blockade treatment in
928 non-small-cell lung cancer. *Annals of Oncology.* 2019;30:1311-20.
- 929 52. Biton J, Mansuet-Lupo A, Pécuchet N, Alifano M, Ouakrim H, Arrondeau J, et
930 al. TP53, STK11, and EGFR Mutations Predict Tumor Immune Profile and the
931 Response to Anti-PD-1 in Lung Adenocarcinoma. *Clin Cancer Res.*
932 2018;24:5710-23.

933

934 **Figure legends**

935 **Fig 1: CD8⁺ T cell-dependent immunity is responsible for the inhibitory effect of**
936 **EGFR-TKI on tumor growth in *Egfr*-mutant lung cancer.**

937 **A.** Left: NanoString analysis on lungs from wild-type mice (n=4 lungs. 4 mice per
938 group.) and genetically engineered mice bearing tumors with the *Egfr* exon 19 deletion
939 (n=4 lungs. 4 mice per group.) were assessed. Right: Relative gene expression score
940 related to immune cell function between the lungs from wild-type and genetically
941 engineered mice harboring *Egfr* exon 19 deletion. Benjamini-Hochberg procedure was
942 used to control the False Discovery Rate at 0.05. **B.** Left: Syngeneic *Egfr*-mutant lung
943 cancer mouse model treated with EGFR-TKI, gefitinib or saline with 0.5%
944 polyoxyethylene sorbitan monooleate as vehicle for 3 days. Right: Effect of gefitinib
945 (50 mg/kg, p.o.) or vehicle control on tumor growth in the *Egfr*-mutant lung cancer
946 model over 3 days. n = 6 tumors per group. 3 mice per group. Data shown are
947 representative of 3 independent experiments with similar results. **C.** Cytokine array on
948 *Egfr*-mutant lung tumors from mice treated with gefitinib (50 mg/kg) or vehicle for 3
949 days. **D.** Representative images of CD8 and Foxp3 IHC staining on *Egfr*-mutant lung
950 tumors from mice treated with vehicle or gefitinib (50 mg/kg) for 3 days..
951 Magnification: ×200 or ×800. Bars: 100 μm. Data shown are representative of 3

CD8⁺ T cell-dependent response in *Egfr*-mutant lung cancer

952 independent experiments with similar results. **E.** FCM analysis of CD8⁺ T cells
953 (CD3⁺CD8⁺; left) and Tregs (CD4⁺CD25⁺FOXP3⁺; center) infiltrating *Egfr*-mutant lung
954 tumors. n=6 tumors per group. 3 mice per group. The CD8⁺ T-cell/Treg ratio (right)
955 was then calculated. Data shown are representative of 3 independent experiments with
956 similar results. **F.** Tumor growth in the *Egfr*-mutant lung cancer model. Mice were
957 treated with gefitinib (50 mg/kg, p.o., 7 days/week) for 14 days with/without CD8⁺ T-
958 cell depletion and subsequently observed for 14 days. Isotype antibody (n=6 tumors per
959 group. 3 mice per group) and anti-CD8 (n=6 tumors per group. 3 mice per group). Data
960 shown are representative of 2 independent experiments with similar results. **G.** Tumor
961 growth in the *Egfr*-mutant lung cancer model without gefitinib treatment with/without
962 CD8⁺ T-cell depletion. Isotype antibody (n=6 tumors per group. 3 mice per group) and
963 anti-CD8 (n=6 tumors per group. 3 mice per group). Bars, mean±standard error. ns, not
964 significant. **p<0.01, ***p<0.001, ****p<0.0001, t-test. Ab, antibody.

965

966 **Fig 2: Combination effect of the EGFR-TKI and anti-PD-1 on the TME and tumor**
967 **growth in *Egfr*-mutant lung cancer.**

968 **A.** FCM analysis of PD-1⁺CD8⁺ T cells infiltrating *Egfr*-mutant lung tumor cells after 3
969 days of treatment with EGFR-TKI (gefitinib, 50 mg/kg, p.o.). n=6 tumors per group. 3

CD8⁺ T cell-dependent response in *Egfr*-mutant lung cancer

970 mice per group. Data shown are representative of 3 independent experiments with
971 similar results. **B.** Representative images of PD-L1 and PD-L2 IHC staining in the *Egfr*-
972 mutant lung tumors after 3 days of treatment with gefitinib (50 mg/kg, p.o.).
973 Magnification: $\times 200$ or $\times 800$. Bars: 100 μm . Data shown are representative of 2
974 independent experiments with similar results. **C.** FCM analysis of PD-L1 and PD-L2 on
975 MC-38 cells or *Egfr*-mutant lung cancer cells treated with IFN γ , IFN α , or vehicle as
976 DMEM. IFN γ : 1×10^2 U/mL for 24 hours; IFN α : 5×10^2 U/mL for 24 hours. Data shown
977 are representative of 2 independent experiments with similar results. **D.** Tumor growth
978 in the *Egfr*-mutant lung cancer model treated with anti-PD-1 (10 mg/kg/day, i.p., every
979 5 days) or isotype control for 17 days. Isotype antibody group (n=5 tumors per group,
980 n=5 mice per group) and anti-PD-1 group (n=5 tumors per group, 5 mice per group).
981 The tumors were subcutaneously transplanted into the single flank of each mice. **E.**
982 FCM analysis of CD8⁺ T cells (left) and Tregs (center) infiltrating *Egfr*-mutant lung
983 tumors treated with anti-PD-1 (10 mg/kg/day, i.p.) or isotype control. The CD8⁺ T-
984 cell/Treg ratio (right) was then calculated. n=6 tumors per group. 3 mice per group.
985 Data shown are representative of 3 independent experiments with similar results. **F.**
986 Tumor growth in the *Egfr*-mutant lung cancer model treated with EGFR-TKI (gefitinib,
987 50 mg/kg, p.o., 5 days/week) and anti-PD-1 or isotype control for 14 days and

CD8⁺ T cell-dependent response in *Egfr*-mutant lung cancer

988 subsequently observed for 14 days. Isotype antibody (n=6 tumors per group. 3 mice per
989 group); anti-PD-1 (n=6 tumors per group. 3 mice per group). Data shown are
990 representative of 3 independent experiments with similar results. **G.** FCM analysis of
991 CD8⁺ T cells (left) and Tregs (center) infiltrating *Egfr*-mutant lung tumors that were
992 treated with EGFR-TKI (gefitinib, 50 mg/kg, p.o.) or combination with anti-PD-1 (10
993 mg/kg/day, i.p.). The CD8⁺ T-cell/Treg ratio (right) was then calculated. n=6 tumors per
994 group. 3 mice per group. Data shown are representative of 2 independent experiments
995 with similar results. Bars, mean±standard error. ns, not significant. ***p<0.001,
996 ****p<0.0001, t-test. *Egfr* mt, *Egfr*-mutated lung cancer cells; Ab, antibody; Comb.,
997 combination EGFR-TKI/anti-PD-1.

998

999 **Fig 3: Combination effect of the EGFR-TKI and anti-VEGFR2 on the TME and**
1000 **tumor growth in *Egfr*-mutant lung cancer.**

1001 **A.** Representative images of CD31 IHC staining in *Egfr*-mutant lung tumors after 3
1002 days of treatment with EGFR-TKI (gefitinib, 50 mg/kg, p.o. 5 days/week), anti-
1003 VEGFR2 (10 mg/kg/day, i.p. every 3 days), combination EGFR-TKI/anti-VEGFR2, or
1004 saline with 0.5% polyoxyethylene sorbitan monooleate as the vehicle control. n=6
1005 tumors per group. 3 mice per group. Data shown are representative of 2 independent

CD8⁺ T cell-dependent response in *Egfr*-mutant lung cancer

1006 experiments with similar results. Magnification: $\times 200$ or $\times 800$. Bars: 100 μm . **B.** Tumor
1007 growth in the *Egfr*-mutant lung cancer model treated with anti-VEGFR2 (10 mg/kg/day,
1008 i.p., every 3 days) or isotype control for 7 days. Isotype antibody (n=4 tumors per
1009 group. 2 mice per group); anti-VEGFR2 (n=6 tumors per group. 3 mice per group). Data
1010 shown are representative of 3 independent experiments with similar results. **C-D.**
1011 Representative images of CD8 and Foxp3 IHC staining in the *Egfr*-mutant lung cancer
1012 tumors after 3 days of treatment with EGFR-TKI (gefitinib, 50 mg/kg, p.o., 5
1013 days/week), anti-VEGFR2 (10 mg/kg/day, i.p., every 3 days), combination EGFR-
1014 TKI/anti-VEGFR2, or saline with 0.5% polyoxyethylene sorbitan monooleate as the
1015 vehicle control. Magnification: $\times 200$ or $\times 800$. Bars: 100 μm . Data shown are
1016 representative of 2 independent experiments with similar results. **E.** FCM analysis of
1017 CD8⁺ T cells (left) and Tregs (center) infiltrating *Egfr*-mutant lung tumors treated with
1018 anti-VEGFR2 (10 mg/kg/day, i.p.) or isotype control every 3 days. The CD8⁺ T-
1019 cell/Treg ratio (right) was then calculated. n=6 tumors per group. 3 mice per group.
1020 Data shown are representative of 2 independent experiments with similar results. **F.**
1021 Tumor growth in the *Egfr*-mutant lung cancer model treated with EGFR-TKI (gefitinib,
1022 50 mg/kg, p.o., 5 days/week) and anti-VEGFR2 (10 mg/kg/day, i.p., every 3 days) or
1023 isotype control for 14 days and subsequently observed for 14 days. Isotype antibody

CD8⁺ T cell-dependent response in *Egfr*-mutant lung cancer

1024 (n=6 tumors per group. 3 mice per group); anti-VEGFR2 (n=6 tumors per group. 3 mice
1025 per group). Data shown are representative of 3 independent experiments with similar
1026 results. **G.** FCM analysis of CD8⁺ T cells (left) and Tregs (center) infiltrating *Egfr*-
1027 mutant lung tumors treated EGFR-TKI (gefitinib, 50 mg/kg, p.o., 5 days/week) or
1028 combination EGFR-TKI/anti-VEGFR2 (10 mg/kg/day, i.p., every 3 days) for 3 days.
1029 The CD8⁺ T-cell/Treg ratio (right) was then calculated. n=6 tumors per group. 3 mice
1030 per group. Data shown are representative of 2 independent experiments with similar
1031 results. Bars, mean±standard error. ns, not significant. *p<0.05, **p<0.01,
1032 ****p<0.0001, t-test. Ab, antibody; Comb., combination EGFR-TKI/anti-VEGFR2.

1033

1034 **Fig 4: Combination effect of anti-PD-1 and anti-VEGFR2 on the TME and tumor**
1035 **growth in *Egfr*-mutant lung cancer.**

1036 **A.** Tumor growth in the *Egfr*-mutant lung cancer model treated with combination of
1037 anti-PD-1 (10 mg/kg/day, i.p., per 5 days) or combination anti-PD-1/anti-VEGFR2 (10
1038 mg/kg/day, i.p., every 3 days) for 10 days. anti-PD-1 (n=4 tumors per group. 2 mice per
1039 group); combination (n=6 tumors per group. 3 mice per group). **B.** FCM analysis of
1040 CD8⁺ T cells (left) and Tregs (center) infiltrating *Egfr*-mutant lung tumors treated with
1041 anti-PD-1 (10 mg/kg/day, i.p., per 5 days) or combination anti-PD-1/anti-VEGFR2 (10

1042 mg/kg/day, i.p., every 3 days) for 3 days. The CD8⁺ T-cell/Treg ratio (right) was then
1043 calculated. n=6 tumors per group. 3 mice per group. Data shown are representative of 2
1044 independent experiments with similar results. Bars, mean±standard error. ns, not
1045 significant, t-test. Ab, antibody; Comb., combination anti-PD-1/anti-VEGFR2.

1046

1047 **Fig. 5: Subsequential combination effect anti-PD-1 and anti-VEGFR2 on tumor**
1048 **growth in *Egfr*-mutant lung cancer with prior EGFR-TKI treatment.**

1049 **A.** Representative images of CD8 and Foxp3 IHC staining in *Egfr*-mutant lung tumors
1050 treated with EGFR-TKI (gefitinib, 50 mg/kg, p.o., 7 days/week) for 3 or 14 days. Data
1051 shown are representative of 3 independent experiments with similar results.
1052 Magnification: ×200 or ×800. Bars: 100 μm. **B.** FCM analysis of the CD8⁺ T-cell/Treg
1053 ratio in *Egfr*-mutant lung tumors after 3 or 14 days of EGFR-TKI treatment. n=5-6
1054 tumors per group. 3 mice per group. Data shown are representative of 2 independent
1055 experiments with similar results. ***p<0.001, t-test. **C.** FCM analysis of PD-1⁺CD8⁺ T
1056 cells in *Egfr*-mutant lung tumors after 3 or 14 days of EGFR-TKI treatment. n=6 tumors
1057 per group. 3 mice per group. Data shown are representative of 2 independent
1058 experiments with similar results. ****p<0.0001, t-test. **D.** Schematic image of the
1059 treatment schedule. (1) prior EGFR-TKI treatment for 14 days (2) sequential therapies

CD8⁺ T cell-dependent response in *Egfr*-mutant lung cancer

1060 as indicated for 7 days. (3) observation period for 14 days. **E.** Tumor growth in the
1061 *Egfr*-mutant lung cancer model (mice from D) treated with EGFR-TKI (gefitinib, 50
1062 mg/kg, p.o., 7 days/week) for 14 days, followed by treatment with anti-PD-1, anti-
1063 VEGFR2, or combination anti-PD-1/anti-VEGFR2 for 7 days and subsequently
1064 observed for 14 days. Isotype control (n=6 tumors per group. 3 mice per group), anti-
1065 VEGFR2 (10 mg/kg/day, i.p., every 3 days; n=6 tumors per group. 3 mice per group),
1066 anti-PD-1 (10 mg/kg/day, i.p. every 5 days; n=6 tumors per group. 3 mice per group),
1067 combination anti-PD-1/anti-VEGFR2 (n=6 tumors per group. 3 mice per group). Data
1068 shown are representative of 2 independent experiments with similar results. *p<0.05,
1069 one-way ANOVA with post-hoc Tukey's test. **F. H.** Survival of mice from E or G was
1070 calculated using the Kaplan–Meier method, and differences in survival were evaluated
1071 using the log-rank test. Kaplan–Meier plot shows percentage of animals with tumor
1072 burden below 500% compared to those at Day 14 for the duration of this study. n=6
1073 tumors per group. 3 mice per group. Data shown are representative of 2 independent
1074 experiments with similar results. *p<0.05, **p<0.01, Log-rank test with Bonferroni
1075 correction (**F**), Log-rank test (**H**). **G.** Tumor growth in the *Egfr*-mutant lung cancer
1076 model treated with EGFR-TKI (gefitinib, 50 mg/kg, p.o., 7 days/week) for 14 days and
1077 subsequent combination anti-PD-1 (10 mg/kg/day, i.p., every 5 days) and anti-VEGFR2

CD8⁺ T cell-dependent response in *Egfr*-mutant lung cancer

1078 (10 mg/kg/day, i.p., every 3 days). Isotype antibody (n=6 tumors per group. 3 mice per
1079 group); anti-CD8 (n=6 tumors per group. 3 mice per group). Data shown are
1080 representative of 2 independent experiments with similar results. *p<0.05, t-test. Bars,
1081 mean±standard error. ns, not significant. Ab, antibody; Comb., combination anti-PD-
1082 1/anti-VEGFR2; Iso, isotype.

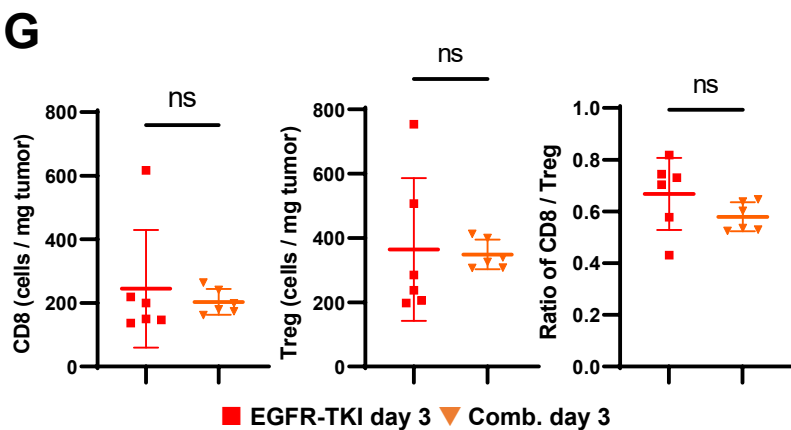
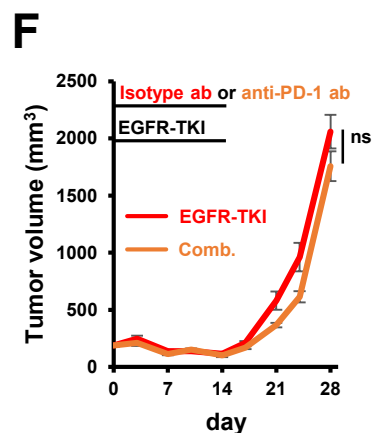
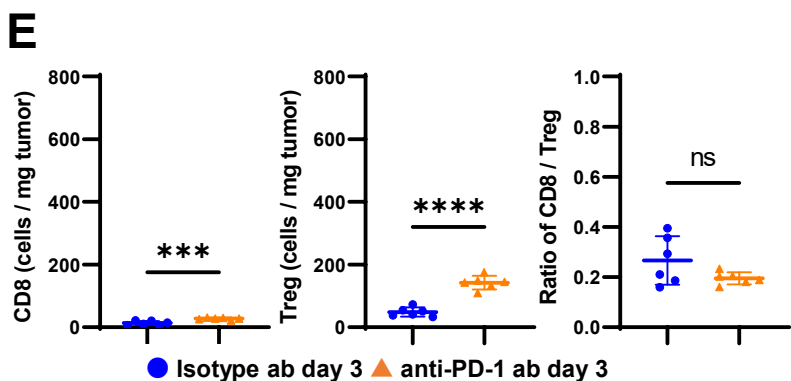
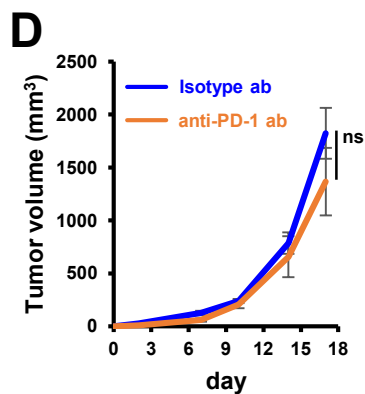
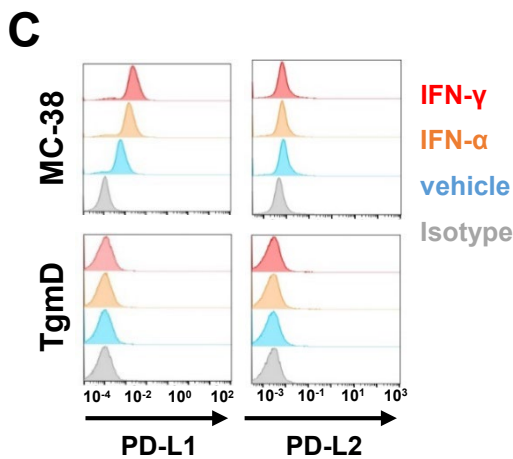
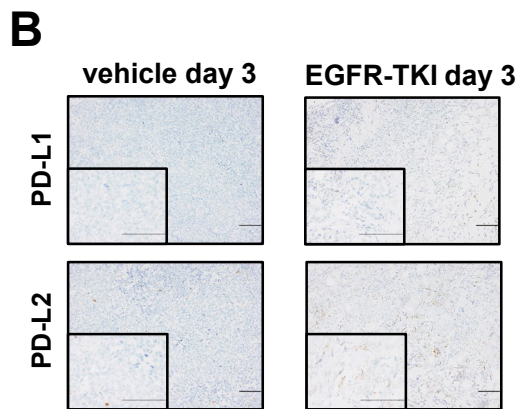
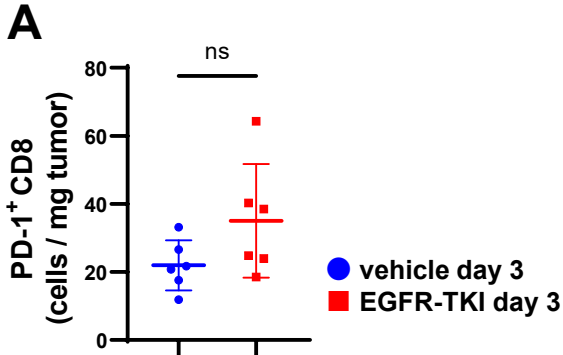
1083

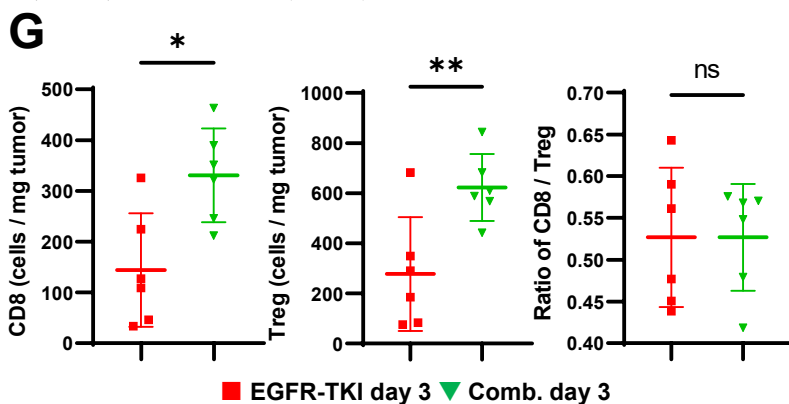
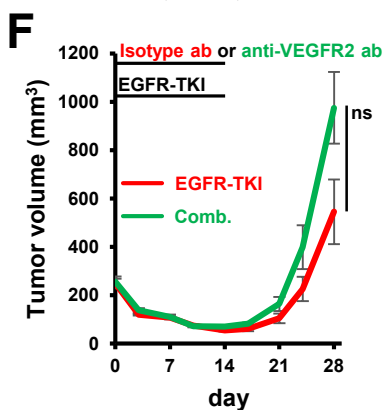
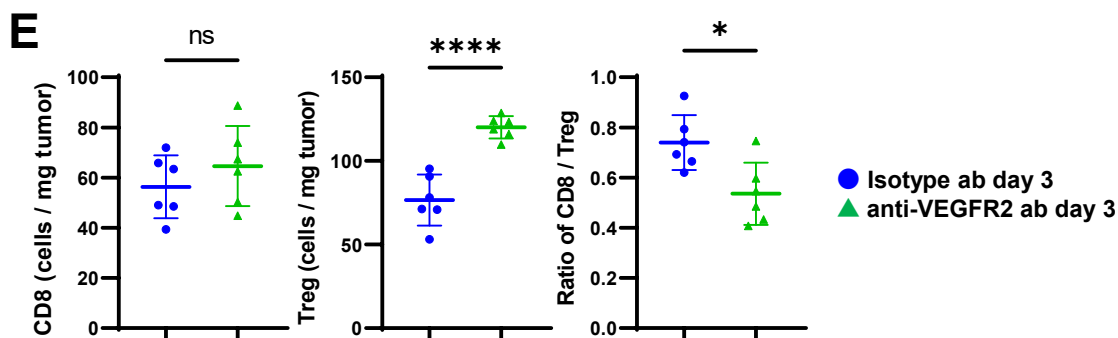
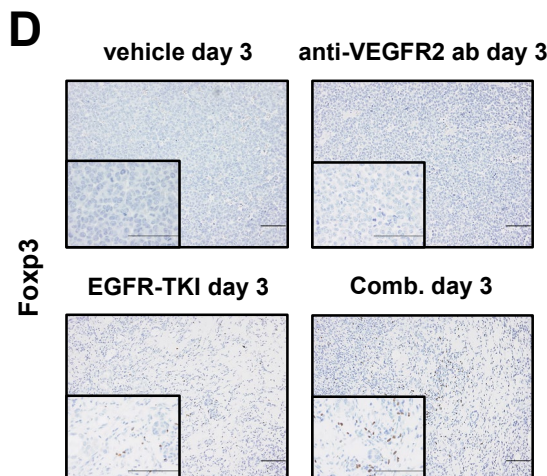
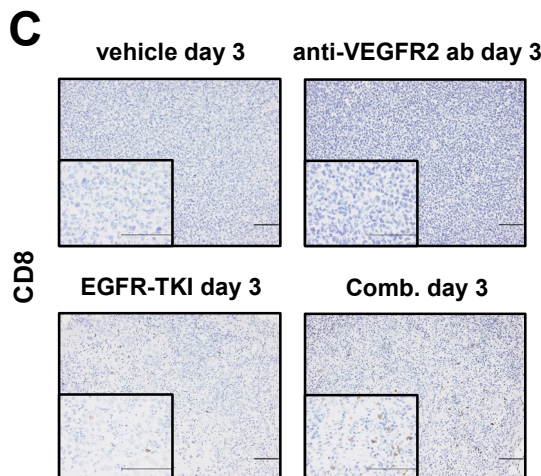
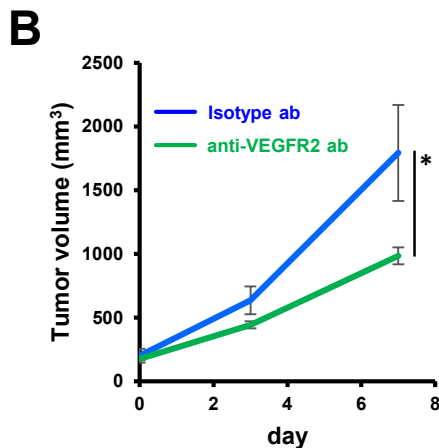
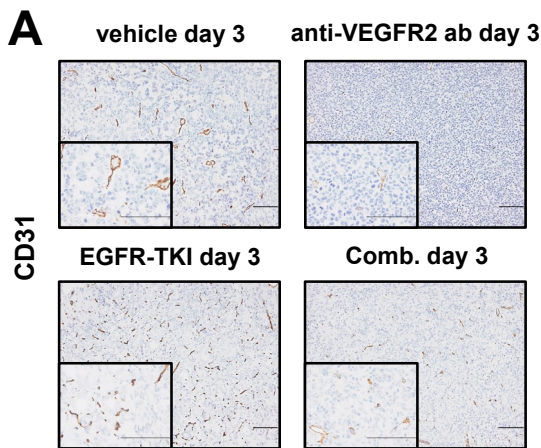
1084 **Fig. 6: Sustained effect of subsequential combination of anti-PD-1 and anti-**
1085 **VEGFR2 on the TME in *Egfr*-mutant lung cancer with prior EGFR-TKI**
1086 **treatment.**

1087 **A.C.F.** Representative images of CD8, CD11c, and Foxp3 IHC staining in *EGFR*-
1088 mutant lung tumors at Day 21 post treatment with isotype antibody, anti-PD-1, anti-
1089 VEGFR2, or combination anti-PD-1/anti-VEGFR2. Data shown are representative of 2
1090 independent experiments with similar results. Magnification: ×200 or ×800. Bars: 100
1091 μm. **B.D.G.** The CD8⁺, CD11c⁺, and Foxp3⁺ areas were quantified using ImageJ
1092 software. Data shown are representative of 2 independent experiments with similar
1093 results. Data are presented as the mean±S.E. (n=5 field-of-view per group,
1094 Magnification: ×200). Bars, mean±standard error. ns, not significant. *p<0.05,
1095 ***p<0.001, ****p<0.0001, one-way ANOVA with post-hoc Tukey's test. **E. *Ccl19***

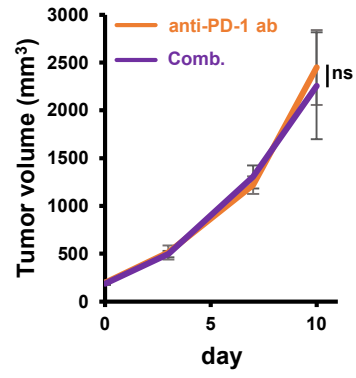
CD8⁺ T cell-dependent response in *Egfr*-mutant lung cancer

1096 RNA expression in the tumors treated with saline with 0.5% polyoxyethylene sorbitan
1097 monooleate as vehicle for 3 days or indicated drugs at 3, 14 and 21 days. Comb.,
1098 combination anti-PD-1/anti-VEGFR2; gef, gefitinib (50 mg/kg 7 days/week); d, days;
1099 gef14d-vehicle D21, gefitinib for 14 days followed by isotype antibody for 7 days;
1100 gef14d-anti-VEGFR2 D21, gefitinib for 14 days followed by anti-VEGFR2 (10
1101 mg/kg/day, i.p., every 3 days) for 7 days; gef14d-anti-PD-1 D21, gefitinib for 14 days
1102 followed by anti-PD-1 (10 mg/kg/day, i.p., per 5 days) for 7 days; gef14d-comb D21,
1103 gefitinib for 14 days followed by combination anti-PD-1/anti-VEGFR2 for 7 days. n=1
1104 tumors per group.
1105
1106





A



B

